Hindawi
Shock and Vibration
Volume 2021, Article ID 7866802, 27 pages
https://doi.org/10.1155/2021/7866802

Research Article

In-Line and Cross-Flow Coupling Vibration Response Characteristics of a Marine Viscoelastic Riser Subjected to Two-Phase Internal Flow

Xueping Chang,[1,2] **Jinming Fan**,[1] **Wenwu Yang**,[1] **and Yinghui Li**[2]

[1]*School of Mechatronic Engineering, Southwest Petroleum University, Chengdu 610500, China*
[2]*School of Mechanics & Engineering, Southwest Jiaotong University, Chengdu 610031, China*

Correspondence should be addressed to Xueping Chang; xuepingch0952@sina.com and Yinghui Li; yhli2007@sina.com

Received 16 March 2020; Revised 17 June 2020; Accepted 7 January 2021; Published 17 February 2021

Academic Editor: Reza Kolahchi

This paper studies the in-line and cross-flow coupling vibration response characteristics of a marine viscoelastic riser subjected to two-phase internal flow and affected by the combined effects of several parameters including the volume fraction of gas phase, sea water flow velocity, viscoelastic coefficient of the marine riser, axial tension amplitude, and the in-line and cross-flow coupling effect taking into account both the geometric and hydrodynamic nonlinearities. On the base of extended Hamilton's principle for open systems, the dynamic equations of the marine viscoelastic riser subjected to the axial tension and gas-liquid-structure interaction are established. Two distributed and coupled van der Pol wake oscillators are utilized to model the fluctuating lift and drag coefficients, respectively. The finite element method is adopted to directly solve the highly coupled nonlinear fluid-structure interaction equations. Model validations are firstly performed through comparisons with the published experimental data and numerical simulation results, and the characteristic curves of the in-line and cross-flow vibration pattern, the in-line and cross-flow displacement trajectories, the in-line and cross-flow space-time response of displacement, and the in-line and cross-flow space-time response of stress versus different parameters are obtained, respectively. The results show that the volume fraction of gas phase, sea water flow velocity, viscoelastic coefficient of marine riser, axial tension amplitude, the in-line and cross-flow coupling effect, and multiphase internal flow velocity have significant influences on the dynamic response characteristics of the marine viscoelastic riser. Furthermore, the maximum displacements and stresses of the marine viscoelastic riser can be increased or decreased depending on the internal flow velocity, and the critical internal flow velocities result in the increase of mode order for different cross-flow velocities. It is also demonstrated that appropriate viscoelastic coefficients are very important to effectively suppress the maximum displacements and stresses.

1. Introduction

Marine risers are indispensable equipment in offshore oil and gas exploitation, which connects the production platform on the surface and the subsea wellhead and provides key transmission channels transporting the drilling fluid or oil and gas. The marine risers are in a complex ocean environment and subjected to the combined actions of multiphase internal flow, its own gravity, the top tension, and a variety of external currents, such as uniform flow and shear flow, which lead to the complex force and make the marine riser have a variety of dynamic problems [1, 2]. Therefore, the marine riser is the weakest and easily damaged component in the offshore drilling platform system. As an important form of fluid-structure interaction response, the vortex-induced vibration (VIV) of the marine riser not only affects the fatigue life of the structure but also, sometimes, directly causes the destruction of the structure due to the large-amplitude oscillation generated by its frequency-locked resonance, which leads to the occurrence of major accidents in offshore oil and gas exploitation [3–5]. At present, the fatigue damage caused by the VIV has become

one of the most serious problems in the dynamics of the marine risers. Consequently, it is urgent to study the VIV responses characteristics of the marine riser systematically and comprehensively.

Over the past several decades, models that predict the response of marine risers have received considerable attention. The majority of research efforts related to the cylinder VIV modeling, simulation, and experiment in the past have been focused on the study of flexibly-mounted rigid cylinders [6–8] and long slender cylinders [9–12]. For rigid cylinders, a new two-degree-of-freedom wake oscillator model was proposed by considering the relative flow velocity around the cylinder [13, 14]. Moreover, geometric nonlinearities are very important to the accurate prediction of response amplitudes and hydrodynamic properties [15, 16]. For flexible long cylinders, many research studies focus on the VIV phenomenon of a flexible pipe by experiments, numerical simulations, and theories. Based on the Euler–Bernoulli beam theory, Srinil and Ricciardi [17, 18] established a vibration model of a marine riser considering the initial state of static equilibrium in the plane and studied the dynamic response of the marine riser under the action of linear shear flow. Subsequently, by simplifying the three-dimensional vibration of the marine riser into a plane model, Srinil [10] studied the dynamic response of the initial plane bending and the response mechanism of vertical pipe under linear shear flow in plane based on the nonlinear theory. Sanaati et al. [19] discussed the influence of simple harmonic tension and axial stiffness on vibration amplitude and suppression characteristic by experiment and analyzed the dynamic response under axial simple harmonic tension through experiments and numerical simulations. Chaplin et al. [20] investigated the VIVs of a vertical tension riser in a stepped current by experiment and revealed that in-line (IL) and cross-flow (CF) displacements had a strong dependence on the modal composition of the motion. Multimode responses and the asymmetry of the bare pipe response in uniform flow were observed by laboratory tests of Xu et al. [21]. Franzini et al. [22] discussed the dynamic responses of a flexible riser subjected to harmonic excitation at the top by experiment and found that the Mathieu instability may simultaneously occur in more than one mode. Considering the phase difference of support motions at two ends of the pipe and a wake oscillator model based on the van der Pol equation to describe the vortex-induced force, He et al. [23] investigated the nonlinear dynamics of a pipe subjected to vortex-induced vibrations and unsynchronized support motions. Employing the van der Pol wake oscillators to simulate the dynamical behavior of the vortex shedding in the wake, Jiang et al. [24] numerically studied the nonplanar vibrations and multimodal responses of pinned-pinned risers under the combined action of internal and shear cross external fluid flows and discussed the effects of the shear parameter on the dynamic responses of the riser. Based on the wake oscillator model, Dai et al. [25] established the response model of pipe conveying fluid under the excitation of simple harmonic transverse acceleration at the top and found the jump of response amplitude and aperiodic phenomena.

The vibration response characteristics of slender structures can be affected by the material properties. In this aspect, extensive researches have been published in the papers. Based on a four-unknown refined integral plate theory and Galerkin's approach, Rahmani et al. [26] investigated the influence of different boundary conditions on the bending and free vibration behavior of functionally graded sandwich plates resting on a two-parameter elastic foundation. On the basis of a novel integral first-order shear deformation theory, Bousahla et al. [27] investigated the buckling and vibrational behavior of the composite beam armed with single-walled carbon nanotubes resting on Winkler–Pasternak elastic foundation by applying Hamilton's principle and the Navier solution and presented several parametric studies and their discussions. Considering a new type of quasi-3D hyperbolic shear deformation theory and defined material properties by rule of the mixture with an additional term of porosity in the through-thickness direction, Kaddari et al. [28] studied the statics and free vibration of functionally graded porous plates resting on elastic foundations and discussed the influences of the porosity parameter, power-law index, aspect ratio, thickness ratio, and the foundation parameters on bending and vibration of a porous FG plate. Based on a simple quasi-3D hyperbolic theory and four different patterns of porosity variations, Addou et al. [29] investigated the effect of the Winkler/Pasternak/Ken foundation and porosity on the dynamic behavior of FG plates and discussed the influences of gradient index, porosity parameter, stiffness of foundation parameters, mode numbers, and geometry on the natural frequencies of imperfect FG plates. Considering exponential and power-law distributions of the functionally graded beam, applying a hyperbolic shear deformation theory, Chaabane et al. [30] studied the static and dynamic behaviors of functionally graded beams resting on the elastic foundation. Employing a quasi-3D hyperbolic shear deformation model, Boulefrakh et al. [31] investigated bending and dynamic behavior of functionally graded plates resting on visco-Pasternak foundations and discussed the effects of material index, elastic foundation type, and damping coefficient of the foundation, on the bending and dynamic behavior of rectangular functionally graded plates. Considering a simple quasi-3D higher shear deformation theory and the stretching effect, Boukhlif et al. [32] presented a dynamic investigation of functionally graded plates resting on an elastic foundation. Reference [33] presented a finite element formulation for transient dynamic analysis of sandwich beams with embedded viscoelastic material, and the results illustrated that the model had a good agreement with experimental data. Reference [34] proposed and investigated a concept to suppress vibrations of steel catenary risers by using viscoelastic sandwich layers, and a great increase of damping was observed. However, insights into the fully coupled CF, IL and axial (AX) VIV of a marine riser considering material viscoelasticity are still lacking in the literature. Therefore, the present research aims at overcoming such model limitation by considering three-dimensional dynamic responses of a marine viscoelastic riser.

The effects of internal flow on the VIV dynamic response of the pipe have been investigated by several researchers. References [35–37] had dedicated to investigate the VIV dynamic responses of a flexible fluid-conveying riser. Furthermore, Reference [38] examined cross-flow (CF) VIV of a flexible fluid-conveying pipe which internal velocities are from subcritical to supercritical. A marine riser often carries a mixture of multiphase energy sources such as oil and gas; therefore, it is important to study the vibration characteristics and instability of the marine riser with multiphase internal flow. Although the dynamics of single-phase pipe conveying fluid had been well studied, the dynamic behaviors of the marine riser subjected to multiphase internal flow need further research. The multiphase flow may lead to differences in material properties, phase-change process, and the excessive turbulence. So far, there has been very little research conducted on the dynamic behavior of marine risers transporting multiphase internal flow. Pettigrew and Taylor [39] reviewed the mechanism of vibration caused by two-phase fluid and analyzed the influence of relevant dynamic parameters on vibration. An and Su [40] used generalized integral transformation (GITT) to analyze the dynamic characteristics of flexible risers transporting two-phase internal flow. Based on the generalized integral transformation method, Ma et al. [41] adopted the Timoshenko beam theory to establish the transverse vibration model of a marine riser transporting two-phase internal flow and studied the influence of different size parameters of the riser and two-phase flow characteristics parameters on the response of the riser.

Although there have been various investigations on the dynamic behaviors of the marine riser in the literature, almost no attention has been paid to the in-line and cross-flow coupling vibration response characteristics of a marine viscoelastic riser subjected to two-phase internal flow and the combined effects of the volume fraction of gas phase, sea water flow velocity, viscoelastic coefficient of the marine riser, axial tension amplitude, and the in-line and cross-flow coupling effect taking into account both the geometric and hydrodynamic nonlinearities on vibration response characteristics. In particular, there is a lack of an effective analytical model for the in-line and cross-flow coupling vibration response characteristics of a marine viscoelastic riser under the consideration of the gas-liquid-structure interaction and hydrodynamic nonlinearities.

This paper is concerned with the in-line and cross-flow coupling vibration response characteristics of a marine viscoelastic riser subjected to two-phase internal flow and the combined effects of the volume fraction of gas phase, sea water flow velocity, viscoelastic coefficient of the marine riser, axial tension amplitude, and the in-line and cross-flow coupling effect taking into account both the geometric and hydrodynamic nonlinearities on the dynamic response characteristics of marine viscoelastic riser. First, based on extended Hamilton's principle for open systems, the dynamic equations of a marine viscoelastic riser, which contain the internal flow velocity coupling term, coupling term of two-phase flow, viscous damping force of internal flow, the axial tension, and the gravity of the marine viscoelastic riser, are established. Two distributed and coupled van der Pol wake oscillators are utilized to model the fluctuating lift and drag coefficients, respectively. Then, employing the finite element method, the highly coupled nonlinear equations of the system are solved and the corresponding characteristic equation is obtained. Finally, some numerical results on the in-line and cross-flow dynamic behaviors and response characteristics of the marine viscoelastic riser varied with different parameters of the volume fraction of gas phase, sea water flow velocity, viscoelastic coefficient of the marine riser, and axial tension amplitude are displayed in detail.

2. Dynamic Model

2.1. Model Description. A marine riser is an important channel connecting the subsea wellhead and the floating platform (fixed or movable) near the surface in offshore oil-gas exploration. A classic marine riser system subjected to oil-gas internal flow is shown schematically in Figure 1(a). For a suitable mathematical modeling of the vibration of a composite marine riser transporting oil-gas internal flow, the following assumptions are introduced to describe the motions of the riser and loading status:

(1) The shear strain is neglected owing to the high slenderness, and the effect of temperature on material properties is ignored.

(2) Owing to the effect of the mooring line constraints and dynamic positioning systems, the platform is only allowed to move in the horizontal direction. Hence, the reacting forces at the two ends are considered to be shear and moment and not torsional loads.

The upper end of the composite marine riser is connected with the sea surface floating production platform through a hydraulic tensioner, and the lower end is connected with the riser base through the flexible joint. In this paper, it is assumed that the fully-submerged flexible pipe with length L is perfectly straight at its vertical static equilibrium due to the effective weight. The fluid-conveying marine riser simply supported at both ends is placed within a uniform fluid flow with cross-flow velocity, $U(z)$, aligned with the axial z-direction, as shown in Figure 1(b). The model of a flexible conveying fluid marine riser is modeled by extended Hamilton's principle. It should be noted that the marine riser will vibrate in-line and cross-flow about the section profile in in-line (IL) x, cross-flow (CF) y, and axial (AX) z-direction.

2.2. Kinetic Energy of Internal Flow. The velocity vector of an arbitrary point on the center line of the marine riser can be written as follows:

$$\mathbf{v} = \dot{r}, \tag{1}$$

where the displacement vector $\mathbf{r}$, which actually means the deformed marine riser position vector at any point, is

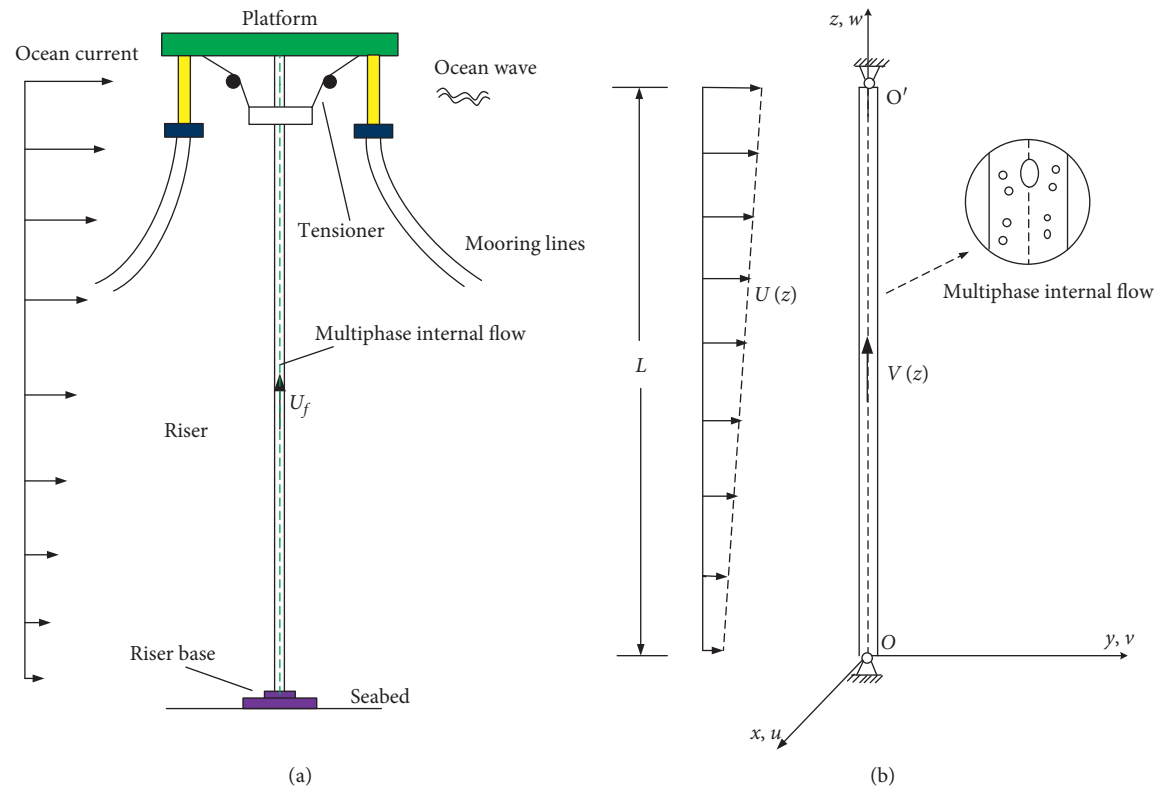

Figure 1: A schematic 3D model of a marine riser system subjected to two-phase internal flow and its simplified model.

$$\mathbf{r} = (u + x)\mathbf{i} + (v + y)\mathbf{j} + (w + z)\mathbf{k}, \tag{2}$$

where $\mathbf{i}$, $\mathbf{j}$, and $\mathbf{k}$ denote the unit vectors along the x-, y- and z-axis. u, v, and w, respectively, denote in-line, cross-flow, and axial displacements, and z is the initial axial coordinate value of the marine riser. Substituting equations (2) to (1), one has

$$\mathbf{v} = \dot{u}\mathbf{i} + \dot{v}\mathbf{j} + \dot{w}\mathbf{k}. \tag{3}$$

According to the schematic diagram of the relative velocity between internal flow and the marine riser, taking the motion of the riser into account, the absolute fluid velocity of the internal fluid element at the same point in the Cartesian coordinate system can be expressed as follows:

$$\mathbf{V}_f = \mathbf{v} + \mathbf{v}_r. \tag{4}$$

Due to the deformation of the marine riser, the relative velocity vector $\mathbf{v}_r$ of the fluid at the center point in the riser cross section is given as

$$\mathbf{v}_r = u'\mathbf{i} + v'\mathbf{j} + (1 + w')\mathbf{k}. \tag{5}$$

Then, substituting equations (3) and (5) into equation (4), the absolute internal fluid velocity $\mathbf{V}_f$ can also be rewritten as follows:

$$\mathbf{V}_f = (\dot{u} + Vu')\mathbf{i} + (\dot{v} + Vv')\mathbf{j} + [\dot{w} + V(1 + w')]\mathbf{k}. \tag{6}$$

It is assumed that the rotary inertia effect and the secondary flow effect are neglected; then, the corresponding kinetic energy T_f of the internal flow can be described as follows:

$$T_f = \frac{1}{2} m_i \int_0^L \left\{ (\dot{u} + Vu')^2 + (\dot{v} + Vu')^2 + [\dot{w} + V(1 + w')]^2 \right\} \mathrm{d}z, \tag{7}$$

where m_i is the mass of the fluid per unit length ($m_i = \rho_i \pi d^2/4$ with ρ_i being the inner fluid density) and V is the internal flow velocity. The over dot (prime) denotes differentiation with respect to time t (axial coordinate z), respectively.

The variation result of kinetic energy of the internal flow is obtained as follows:

$$\begin{aligned}\int_{t1}^{t2}\delta T_f \mathrm{d}t &= \frac{1}{2}m_i\int_{t1}^{t2}\int_0^L \delta\left\{\left(\dot{u}+Vu'\right)^2+\left(\dot{v}+Vu'\right)^2+\left[\dot{w}+V\left(1+w'\right)\right]^2\right\}\mathrm{d}z,\\ &= -\int_{t1}^{t2}\int_0^L m_i\left(\ddot{u}+2V\dot{u}'+V^2u''\right)\delta u\mathrm{d}z\mathrm{d}t-\int_{t1}^{t2}\int_0^L m_i\left(\ddot{v}+2V\dot{v}'+V^2v''\right)\delta v\mathrm{d}z\mathrm{d}t\\ &\quad -\int_{t1}^{t2}\int_0^L m_i\left(\ddot{w}+2V\dot{w}'+V^2w''\right)\delta w\mathrm{d}z\mathrm{d}t.\end{aligned} \tag{8}$$

2.3. Material Viscoelastic Characteristics. In the current work, the pipe material is assumed to be viscoelastic according to the Kelvin–Voigt formulation. Therefore, the relationship between the stress and strain may be expressed as follows:

$$\sigma* = \left(1+\frac{E*}{E}\frac{\partial}{\partial t}\right)E\varepsilon*, \tag{9}$$

where $\sigma*$ and $\varepsilon*$ are the stress and strain, respectively, $E*$ is the coefficient of internal dissipation, and t is the time.

Let $a = E*/E$, and equation (9) can be rewritten as follows:

$$\sigma* = \left(1+a\frac{\partial}{\partial t}\right)E\varepsilon*. \tag{10}$$

2.4. Multiphase Internal Flow Characteristics. It has been observed that the fluid transported in the marine riser always occurs in multiphase flow conditions, and there are several flow regimes in multiphase flow. In this work, we studied a marine riser conveying gas-oil mixtures. Considering different physical properties and flow velocities between different phases, based on Monette et al.'s work [42], m_f, m_fU_f, and $m_fU_f^2$ of the multiphase flow can be written as follows:

$$\begin{aligned}m_f &= \sum_{k=1}^{2} m_{fk},\\ m_fU_f &= \sum_{k=1}^{2} m_{fk}U_{fk},\\ m_fU_f^2 &= \sum_{k=1}^{2} m_{fk}U_{fk}^2.\end{aligned} \tag{11}$$

In order to facilitate the study, it is necessary to define the relevant parameters of two-phase flow in the composite marine riser. ε_g is the gas volume fraction, K is the slip coefficient, and U is the apparent velocity; ε_g, K, and U are, respectively, expressed as

$$\begin{aligned}\varepsilon_g &= \frac{Q_g}{Q_g+Q_l},\\ K &= \frac{U_g}{U_l},\\ U &= \frac{Q_g+Q_l}{A},\end{aligned} \tag{12}$$

where Q_g is the volumetric flow rate of the gas, Q_l is the volumetric flow rate of oil, and the corresponding flow velocity are U_g and U_l, respectively. In addition, the slip coefficient can be expressed as the function of the gas volume fraction, which can be written as $K = [\varepsilon_g/(1-\varepsilon_g)]^{1/2}$.

2.5. Dynamic Equations. Based on Zanganeh and Srinil's work [43], accounting for the effect of multiphase internal flow, and combined with equations (8), (10), and (11) previously derived, it can be shown that the nonlinear partial-differential equations of 3D coupled cross-flow and in-line motions of a marine viscoelastic riser subjected to two-phase internal flow have the forms of

$$\begin{aligned}&\left(m+\sum_{k=1}^{2}m_{ik}+m_a\right)\ddot{u}+c\dot{u}+EIu''''+aEI\dot{u}''''+2\sum_{k=1}^{2}m_{ik}V_k\dot{u}'+\sum_{k=1}^{2}m_{ik}V_k^2u''-\left(Tu'\right)',\\ &=\left(1+a\frac{\partial}{\partial t}\right)EA_r\left(w''u'+w'u''\right)+\frac{1}{2}\left(1+a\frac{\partial}{\partial t}\right)EA_r\left(3u''u'^2+u''w'^2+2w''w'u'+u''v'^2+2v''v'u'\right)+F_x.\end{aligned} \tag{13a}$$

$$\begin{aligned}&\left(m+\sum_{k=1}^{2}m_{ik}+m_a\right)\ddot{v}+c\dot{v}+EIv''''+aEI\dot{v}''''+2\sum_{k=1}^{2}m_{ik}V_k\dot{v}'+\sum_{k=1}^{2}m_{ik}V_k^2v''-\left(Tv'\right)',\\ &=\left(1+a\frac{\partial}{\partial t}\right)EA_r\left(v'w''+v''w'\right)+\frac{1}{2}\left(1+a\frac{\partial}{\partial t}\right)EA_r\left(v''u'^2+2u''u'v'+u''w'^2+v''w'^2+2w''w'v'+3v''v'^2\right)+F_y,\end{aligned} \tag{13b}$$

where F_x and F_y are the associated hydrodynamic forces in three directions, respectively, m is the mass of the marine riser per length, m_i is the internal fluid mass per unit length, and m_a is the additional fluid mass per unit length ($m_a = C_A\rho_o\pi D^2/4$, with C_A being the added mass coefficient and ρ_o being the outer fluid density); it should be noted that the still water added mass coefficient C_A taken as unity for circular cylinder. The parameters related with the marine riser with constant Young's modulus (E), damping coefficient (c), outer diameter (D), inter diameter (d), moment of inertia (I), cross-sectional area (A_r), bending stiffness (EI), and axial stiffness (EA_r).

The static effective tension T without internal flow effect can be spatially varied by accounting for the buoyancy effect; then, the tension of the fluid-conveying pipe can by expressed as follows:

$$T = T_t - g\left(m + m_i - m_a\right)z, \tag{14}$$

where T_t is the top pretension and g is the gravity.

The boundary conditions of the riser are assumed as a simply supported pipe and given by

$$\begin{aligned} u(z,t) &= 0, \\ \frac{\partial^2 u(z,t)}{\partial z^2} &= 0, \\ v(z,t) &= 0, \\ \frac{\partial^2 v(z,t)}{\partial z^2} &= 0, \quad \text{at } z = 0. \end{aligned} \tag{15a}$$

$$\begin{aligned} u(z,t) &= 0, \\ \frac{\partial^2 u(z,t)}{\partial z^2} &= 0, \\ v(z,t) &= 0, \\ \frac{\partial^2 v(z,t)}{\partial z^2} &= 0, \quad \text{at } z = L. \end{aligned} \tag{15b}$$

3. Hydrodynamic Forces

According to the theory of Zanganeh and Srinil [43], the projected three-dimensional hydrodynamic force components can be expressed as

$$\begin{aligned} F_x &= \frac{1}{4}\rho D U_{\text{rel}} C_{l0} q\dot{v} + \frac{1}{4}\rho D U_{\text{rel}} C_{0p} p\left(V - \dot{u}\right) + \frac{1}{2}\rho D U_{\text{rel}} \overline{C}_d p\left(V - \dot{u}\right), \\ F_y &= \frac{1}{4}\rho D U_{\text{rel}} C_{l0} q\left(V - \dot{u}\right) + \frac{1}{4}\rho D U_{\text{rel}} C_{0p} p\dot{v} - \frac{1}{2}\rho D U_{\text{rel}} \overline{C}_d p\dot{v}, \end{aligned} \tag{16}$$

where C_{d0} and C_{l0} are the associated drag and lift coefficients of a stationary cylinder (assumed as $C_{d0} = 0.2$, $C_{l0} = 0.3$, and $\overline{C}_d = 1.2$). The total velocity relative to the pipe can be written as follows:

$$U_{\text{rel}} = U\sqrt{\left(1 - \frac{\dot{u}}{U}\right) + \left(\frac{\dot{v}}{U}\right)^2 + \left(\frac{\dot{w}}{U}\right)^2}. \tag{17}$$

In this paper, the van der Pol nonlinear vibration equations are used to describe the shedding characteristics of vortex, according to the theory of Facchinetti et al. [44], and the variations of p and q can be described as

$$\ddot{p} + 2\varepsilon_u\Omega_f\left(p^2 - 1\right)\dot{p} + 4\Omega_f^2 p = \frac{\Lambda_u}{D}\ddot{u}, \tag{18}$$

$$\ddot{q} + \varepsilon_v\Omega_f\left(q^2 - 1\right)\dot{q} + \Omega_f^2 q = \frac{\Lambda_v}{D}\ddot{v}. \tag{19}$$

Herein, $\Omega_f = 2\pi StU/D$ is the vortex-shedding angular frequency, and the right side of the equations are the excitation terms simulating the effect of pipe motion on the near wake. ε_u, ε_v, Λ_u, and Λ_v are the wake and coupling empirical coefficients adopted equally as $\varepsilon_u = 0.3$, $\Lambda_u = \Lambda_v = 12$, and ε_v calibrated by Zanganeh and Srinil [43].

4. Numerical Results and Discussion

Numerical results are performed in this section to analyze the effects of sea water flow velocity, viscoelastic coefficient of marine riser, axial tension amplitude, multiphase internal flow property, and gas-phase volume fraction on vibration responses characteristics of the marine viscoelastic riser. A long flexible straight riser model experimentally tested by Song et al. [45] can be used for numerical simulations. Geometry parameters and physical property parameters are listed in Tables 1 and 2.

The highly nonlinear partial-differential equations (13a) and (13b) in conjunction with equations (18) and (19) are solved by the FEM in COMSOL program. Initial conditions are specified at the static equilibrium for the marine riser ($u = v = w = \dot{u} = \dot{v} = \dot{w} = 0$), with $p = 2\,(\dot{p} = 0)$ and $q = 2\,(\dot{q} = 0)$ for wake variables. The Lagrange quadratic finite elements are used for the discrete of the riser, and $\Delta t = 0.001$s and $\Delta z = 0.1$ m have been chosen through a series of convergence yielding stable simulations for all considered flow velocities. In this study case, validation tests of numerical simulations with the experimental model and finite difference approach of Zanganeh and Srinil [43] have been performed.

Table 1: Values for geometry parameters of the marine viscoelastic riser.

Geometry and force parameters	Description	Value
L	Length (m)	28.04
D	Outer diameter (m)	0.016
d	Inner diameter (m)	0.015
T	Axial tension (N)	700

Table 2: Values for physical properties parameters of the marine viscoelastic riser.

Physical properties and parameters	Description	Value
ρ_P	Riser density (kg/m^3)	7385
ρ_o	Ocean density (kg/m^3)	1000
ρ_g	Density of gas-phase internal flow (kg/m^3)	1.293
ρ_l	Density of fluid-phase internal flow (kg/m^3)	870
U	Cross-flow velocity (m/s)	0.1–0.3
EI	Bending stiffness (N m^2)	0.02
C	Damping coefficient of the riser	0.001
A	Viscoelastic coefficient	0–0.11

4.1. Validity of the Method and Convergence Verification. Owing to the lack of VIV experiment concerned with internal flow, model validations are firstly performed through comparisons with the published experiment and numerical simulation results. Previous prediction results concluded by Zanganeh and Srinil [43] have highlighted the importance of considering the axial dynamic coupling, the amplification of IL mean displacements, and the geometric and hydrodynamic nonlinearities. Therefore, variations of maximum IL and CF displacement amplitudes of the flexible riser with respect to cross-flow velocity are plotted in Figure 2 for different analysis methods. It is found that the IL displacement amplitudes between experiment and numerical simulations agree very well at lower cross-flow velocity. Outside this region of cross-flow velocity, the IL displacement amplitudes obtained by experiment keep almost larger than numerical simulations.

As for the CF displacement amplitude, it is noted that an increase in the cross-flow velocity results in an increase in the CF displacement amplitude and the peak value of CF displacement amplitude occurs at the cross-flow velocity of around 0.3 m/s for FDM and FEM results. For the maximum displacement, the simulation results are larger than the experimental results. This is because the damping errors of the numerical calculation model in this paper and the experimental model in the references lead to different results, which are related to imperfect physical models and numerical calculation methods. In addition, the boundary conditions are also different, and the upper boundary in the experiment is a spring support, while the upper boundary in the numerical simulation in this paper is a simply supported support. In general, our model can effectively predict the VIV dynamic responses of a flexible riser.

4.2. Influence of Sea Water Velocity on the Vibration Response Characteristics. The influences of sea water flow velocity on the vibration response characteristics of the marine riser considering the in-line and cross-flow coupling effect are discussed in this section.

For some prescribed values of different sea water flow speed, the response characteristic curves of the cross-flow vibration pattern of marine riser versus sea water flow speed with U = 0.1 m/s, 0.3 m/s, 0.5 m/s, and 1.0 m/s are plotted in Figure 3. It can be viewed that the order of the vibration modes of the cross-flow excitation gradually increases with the increase of the sea water flow velocity. When the sea water flow velocity U = 1.0 m/s, it reaches the highest order of 7 in the analysis. Under other flow velocities, the mode order of the marine riser is consistent with that in the figure, except that the cross-flow vibration amplitude is different. However, the even-order modes of the marine riser are not found in the analysis. The reason for this phenomenon is that the characteristic parameters of the marine riser determine that the locking interval of the even-order mode response of the riser under condition that the outflow excitation is small, so it is difficult to capture under several outflow velocities selected in the paper.

Figure 4 shows the phase diagram of the riser when the outflow velocity is 0.3 m/s. Different color curves in the figure represent the phase trajectories along different positions of the riser. Figures 4(a) and 4(b) are the phase diagrams in the downstream direction of the riser, and Figure 4(b) is the partial magnification of Figure 4(a). The results show that the phase diagram in the downstream direction is a closed elliptic ring. However, as can be seen from the partial zoomed-in figure, two intersecting elliptic rings form a closed curve and the riser vibrates twice as periodically in the downstream direction. Figures 4(c) and 4(d) are the cross-flow phase diagrams of the riser, and Figure 4(d) is a partial magnification of Figure 4(c). It can be see that, at a large displacement, the horizontal "8" type appears in the cross-flow phase diagram. At a small displacement, the cross-flow phase diagram shows a circular shape, but the velocity is zero, and there is a large change at the position with the largest displacement. As shown in the

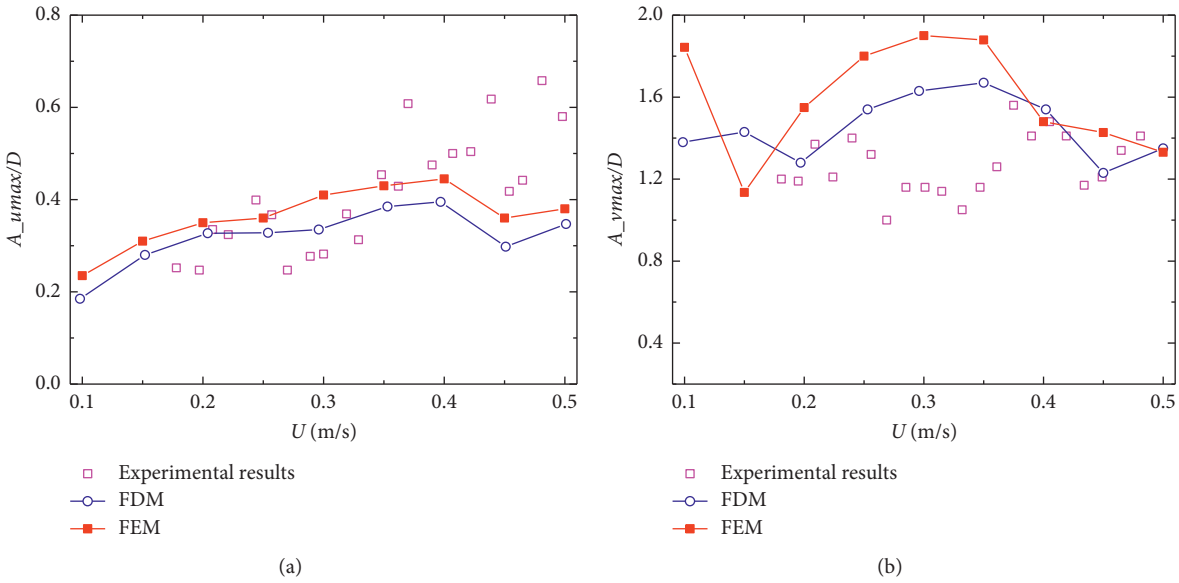

Figure 2: Comparison of maximum displacement amplitudes between the present results and value of experimental measurement of (a) in-line and (b) cross-flow.

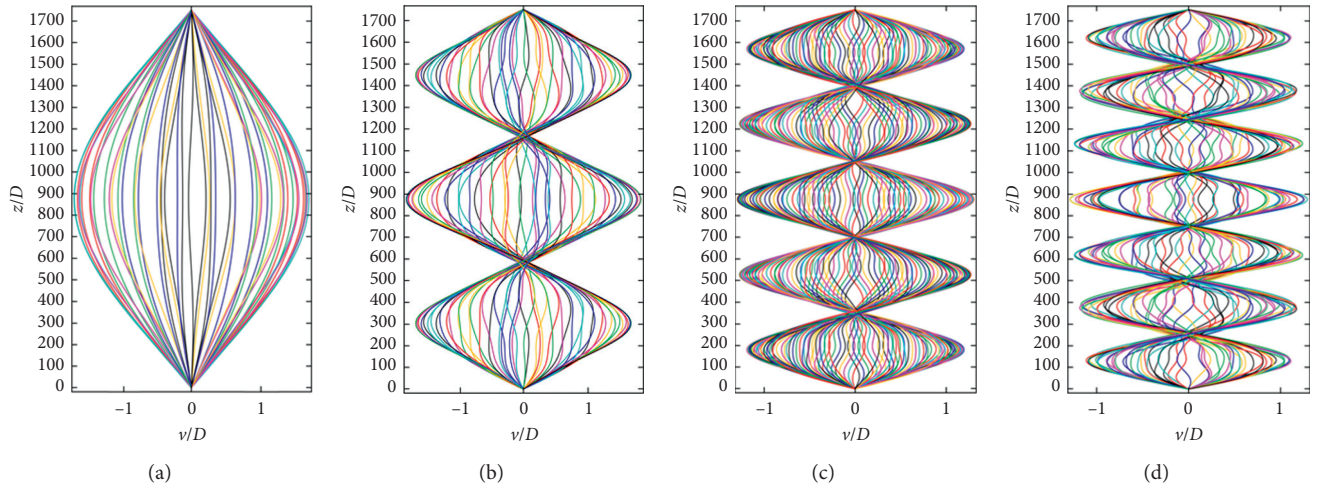

Figure 3: The variations of the cross-flow vibration pattern of the marine riser with different sea water flow speed for (a) $U = 0.1$ m/s, (b) $U = 0.3$ m/s, (c) $U = 0.5$ m/s, and (d) $U = 1.0$ m/s.

local magnification, the cross-flow phase trajectory is a single closed curve without crossing, so the riser shows a single-period vibration in the cross-flow direction.

In Figure 5, the characteristic relationships between stresses and time under different sea water flow velocity are displayed, where Figures 5(a) and 5(c) are the relationships curves of the in-line, while Figures 5(b) and 5(d) are relationships curves of the cross-flow. It is obvious that the stresses closing to the end and middle position of riser are larger, and the in-line bending stress varies near the large stress value with the change of time. In addition, the stress changes in Figure 5(c) along the in-line are more complex, and the stress shows a trend of periodic changes along the axis direction of marine riser.

The relationships curves in Figure 5(b) represent the cross-flow stress change. It can be seen that the cross-flow stresses show a periodic change with time, and the vibration appears as a standing wave form. In addition, the maximum stress and minimum stress alternation happened in three locations. In Figure 5(d), the axial distribution of the maximum stress and minimum stress along the marine riser is more. In addition, the change that stress varies with time is also more complex and characterized by shear wave and standing wave superposition state. The reasons causing the abovementioned phenomenon is that the marine riser vibrates in multiple modes at this velocity.

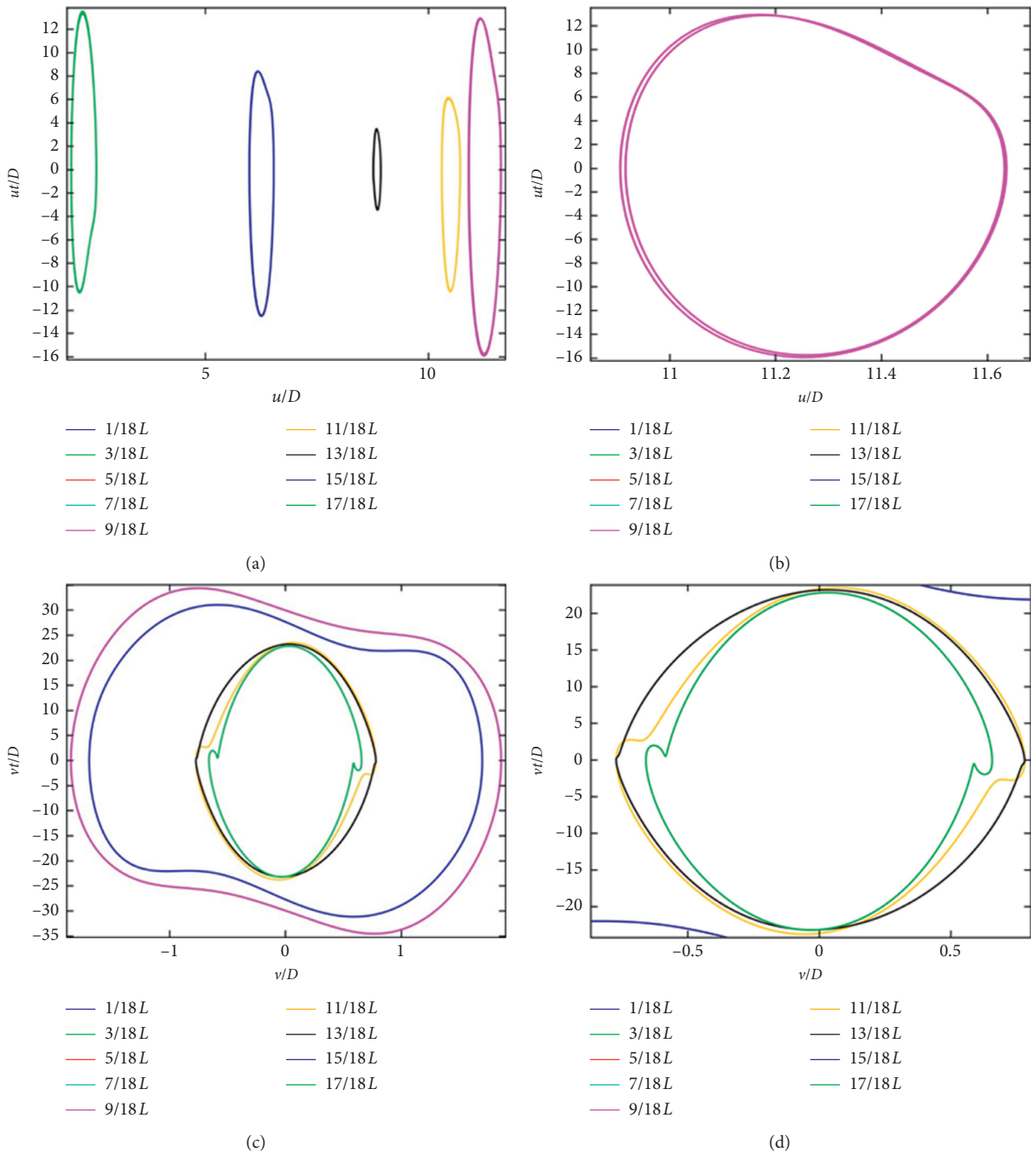

Figure 4: The phase diagram of the marine riser considering the coupling effect: the phase diagram (a) and partial enlargement diagram (b) of the cross-flow and the phase diagram (c) and partial enlargement diagram (d) of the in-line.

4.3. Effects of the Viscoelastic Coefficient on the Vibration Response Characteristics. The influences of the viscoelastic coefficient of the marine riser on the vibration response characteristics considering the in-line and cross-flow coupling effect are discussed in this section. The influences of the viscoelastic coefficient on the low-order frequency of the marine riser are little, while the influences of that on the high-order frequency are great. Moreover, because the viscoelastic term contains time, it shows time-dependent characteristics, so it is necessary to carry out time-domain solution analysis.

For some prescribed values of different sea water flow speeds, the characteristic relationships between time-averaged displacement and viscoelastic coefficients under different flow velocities are displayed in Figure 6, where $U = 0.3$ m/s and $U = 0.8$m/s. It is obvious that the time-averaged displacement in both the in-line and cross-flow decreases with the increase of the viscoelastic coefficient at the condition that $U = 0.3$ m/s. However, the time-averaged displacement in the in-line decreases firstly, then increases, and finally, decreases with the increase of the viscoelastic

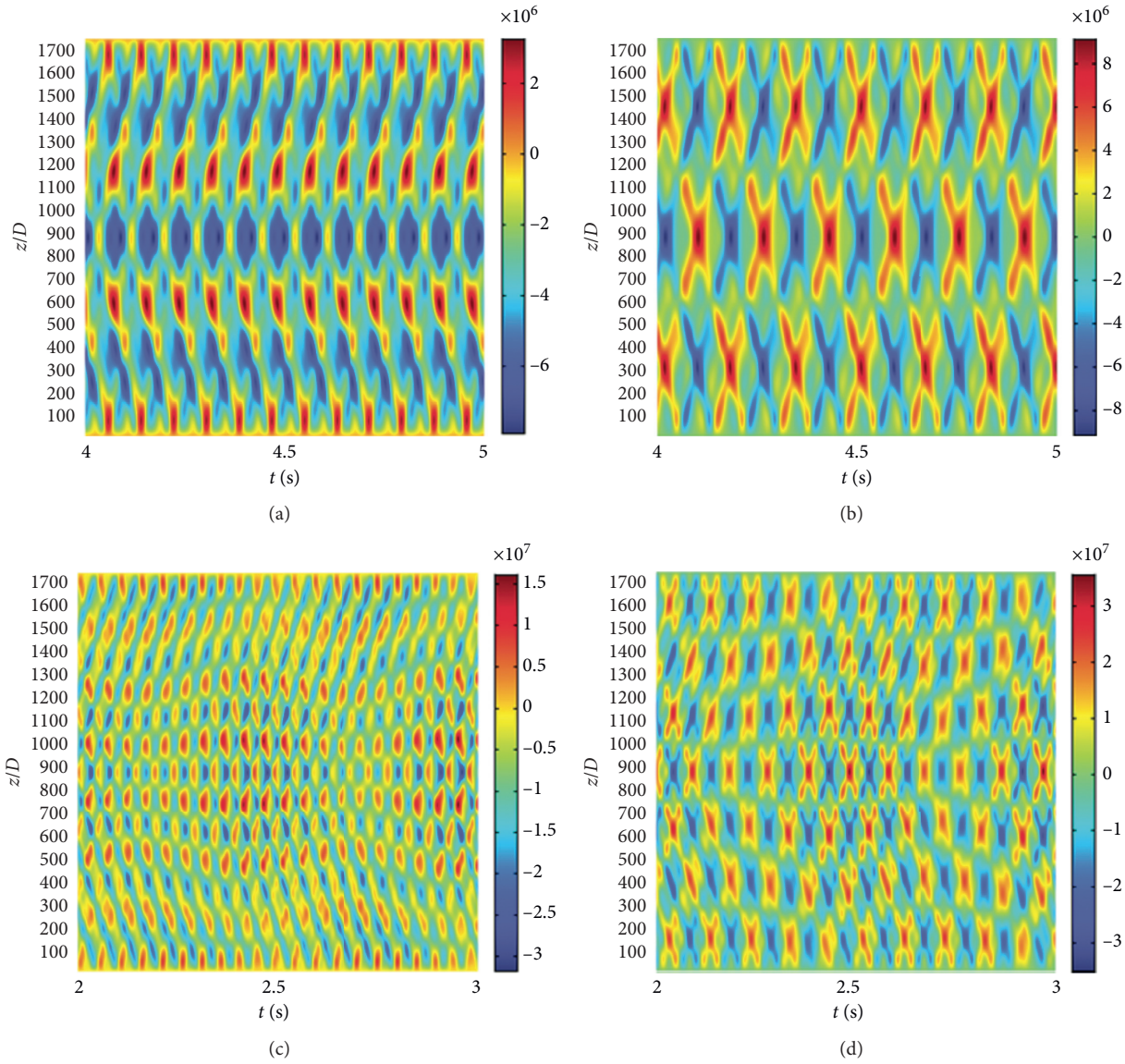

Figure 5: The effects of different sea water velocities on the stress of the marine riser. (a) The in-line and (b) cross-flow with $U = 0.3$ m/s. (c) The in-line and (d) cross-flow with $U = 0.8$ m/s.

coefficient at the condition that $U = 0.8$ m/s, while the time-averaged displacement in the cross-flow increases firstly, then decreases, and finally, increases with the increase of the viscoelastic coefficient at the condition that $U = 0.8$ m/s. The reason causing the abovementioned phenomenon is that the influences of the viscoelastic coefficient on the natural frequency of the marine riser are little and the time-domain response of marine riser is mainly affected by the time effect of the viscoelastic coefficient when the sea water flow velocity is low. However, the influences of the viscoelastic coefficient on the natural frequency of the marine riser are great, and the time-domain response of the marine riser is mainly affected by the natural frequency of the riser and the time effect of the viscoelastic coefficient when the sea water flow velocity is high.

In Figure 7, the characteristic relationship curves of the displacement trajectories of the marine riser with different viscoelastic coefficients are displayed, where the curves in Figures 7(a), 7(c), and 7(e) are the displacement trajectories of the marine riser with $a = 0.001$, while the ones in Figures 7(b), 7(d), and 7(f) are the displacement trajectories of the marine riser with $a = 0.11$. It is obvious that the displacement trajectories in Figure 7(b) are all "8" shaped, while there are double "8-"shaped trajectories near both ends of the riser in Figure 7(a). The phase trajectories in Figures 7(c) and 7(d) are a mixture of "8" shape and "crescent" shape. The phase trajectories near the center of the riser are "crescent" shaped and near both ends of the riser are "8" shaped. The phase trajectories in Figures 7(e) and 7(f) are mainly "8" shaped, while the phase trajectories in Figure 7(e) show double "8-"shaped trajectories at a small downstream displacement.

The space-time response characteristic curves of displacement under different viscoelastic coefficients are

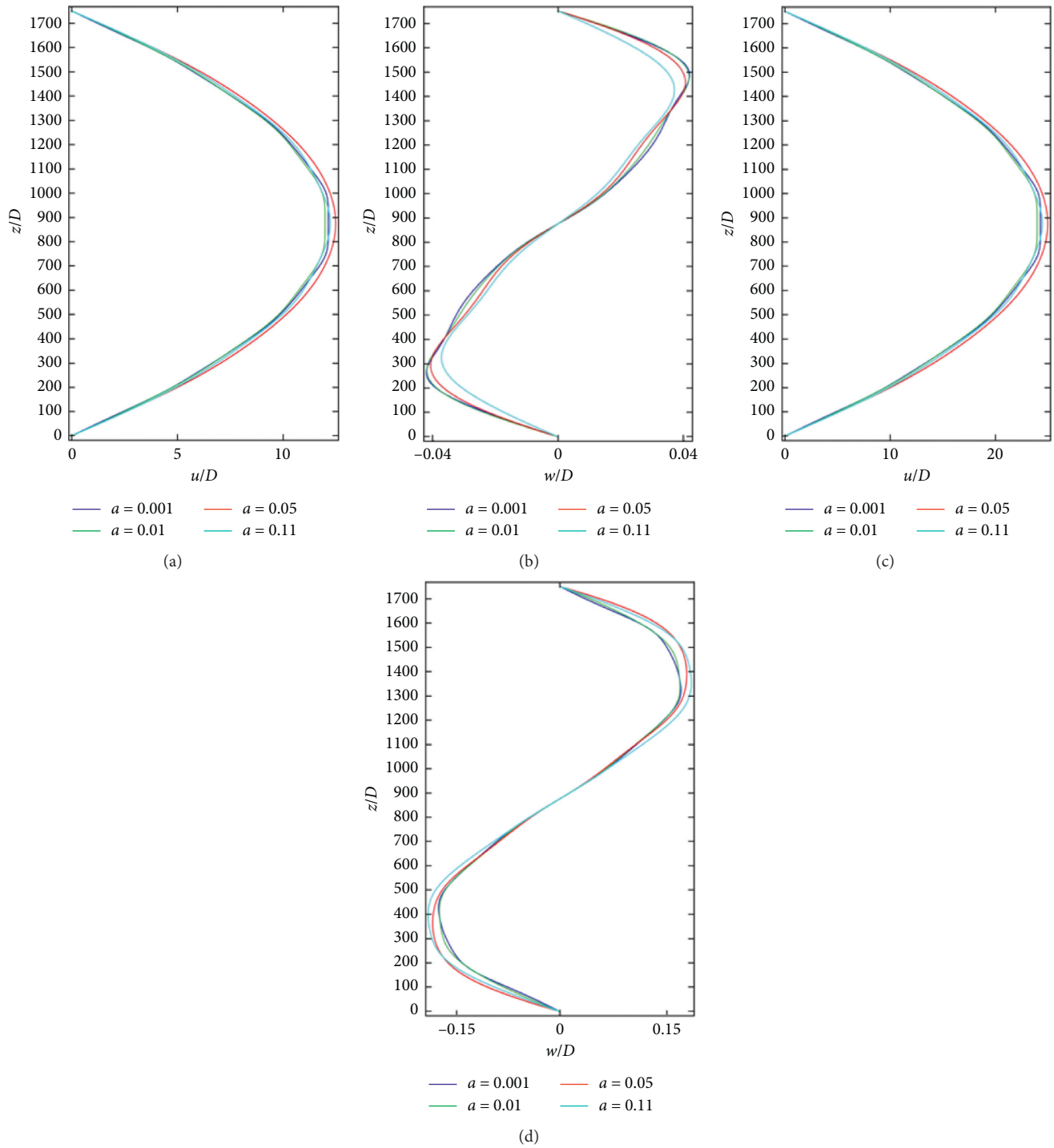

Figure 6: The influences of the viscoelastic coefficient on average displacement at different sea water velocities. (a) and (b) With $U = 0.3$ m/s; (c) and (d) with $U = 0.8$ m/s.

plotted in Figure 8, where Figures 8(a) and 8(b) are displacement responses of the in-line and cross-flow under the condition that $a = 0.001$, respectively, while Figures 8(c) and 8(d) are displacement responses of the in-line and cross-flow under the condition that $a = 0.11$, respectively. It can be viewed that the amplitude of the three-direction maximum displacement decreases with the increase of the viscoelastic coefficient, the space-time variation of the three-direction displacement under different viscoelastic coefficients is similar, and the in-line and cross-flow displacements are symmetrically distributed along the axial direction of the marine riser.

The space-time response characteristic curves of stress under different viscoelastic coefficients are plotted in Figure 9, where Figures 9(a) and 9(b) are stress responses of the in-line and cross-flow under the condition that $a = 0.001$,

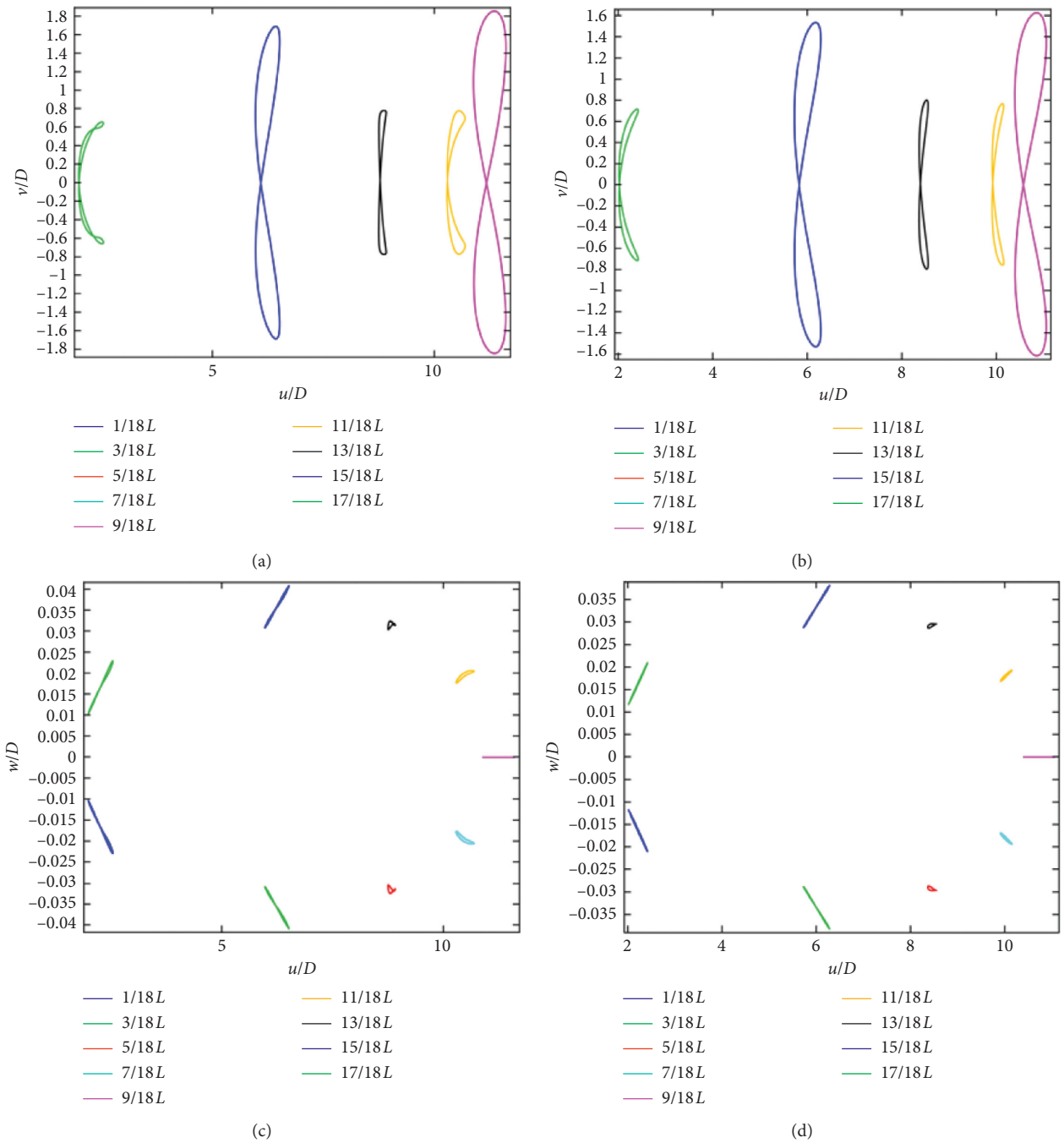

Figure 7: Continued.

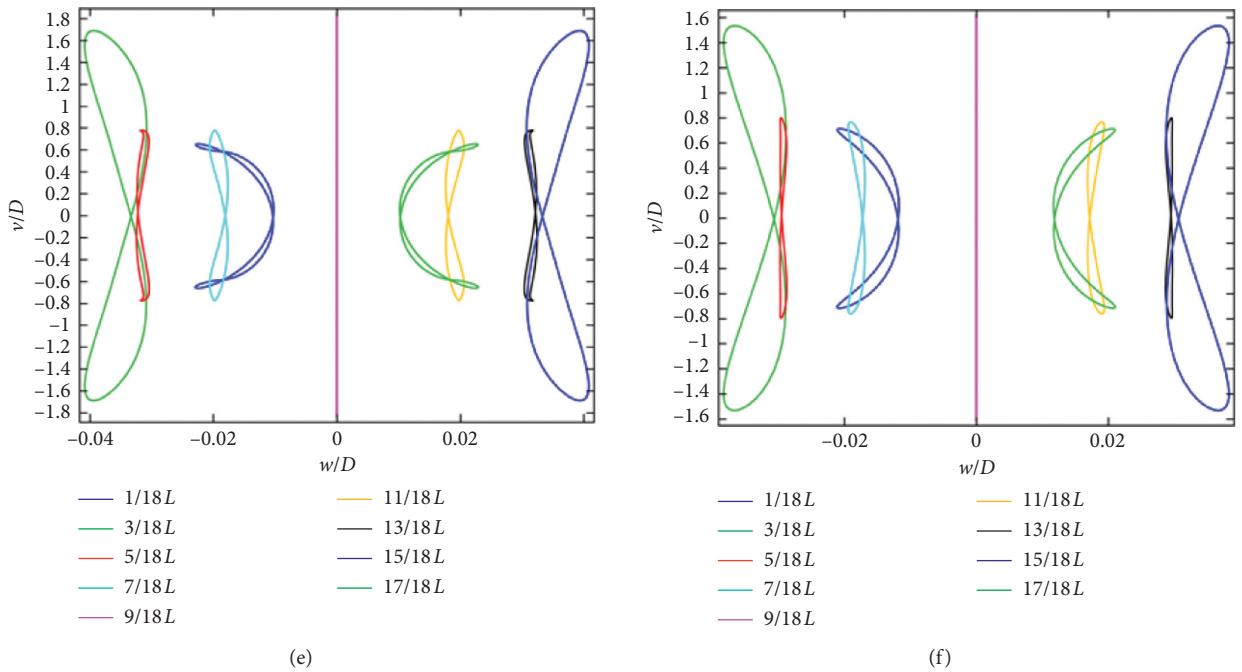

FIGURE 7: The displacement trajectories of the marine riser at different viscoelastic coefficients in the x-y plane with (a) $a = 0.001$ and (b) $a = 0.11$, in the x-z plane with (c) $a = 0.001$ and (d) $a = 0.11$, and in the y-z plane with (e) $a = 0.001$ and (f) $a = 0.11$.

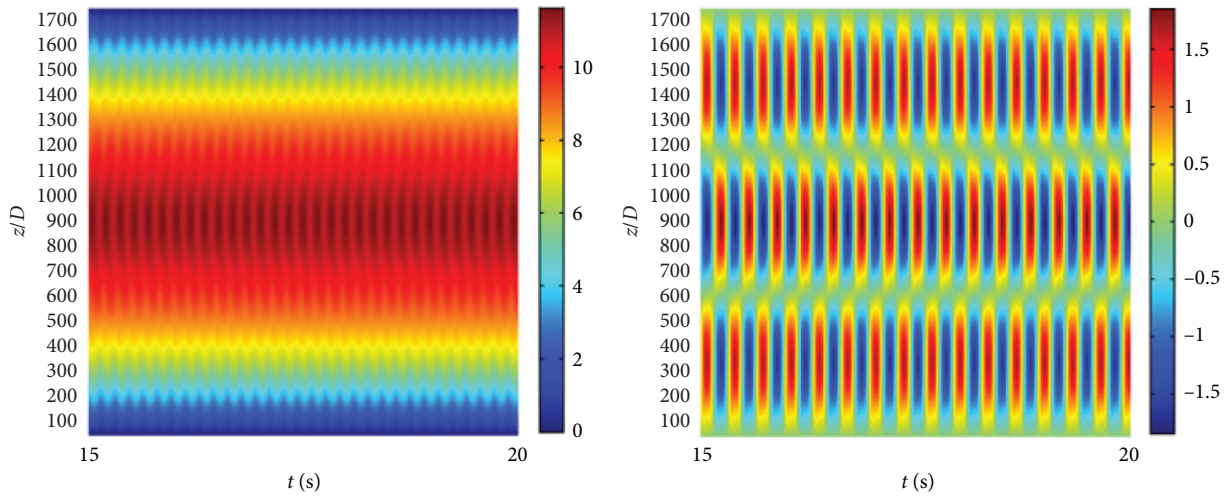

FIGURE 8: Continued.

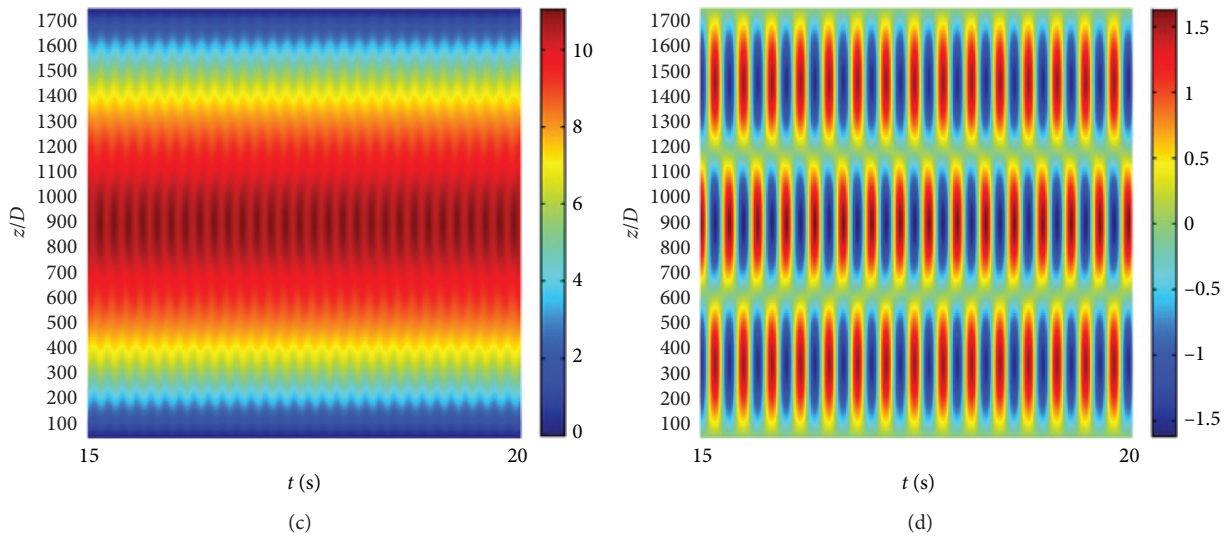

Figure 8: Space-time response of displacement under different viscoelastic coefficients. (a) The in-line and (b) cross-flow with $a = 0.001$. (c) The in-line and (d) cross-flow with $a = 0.11$.

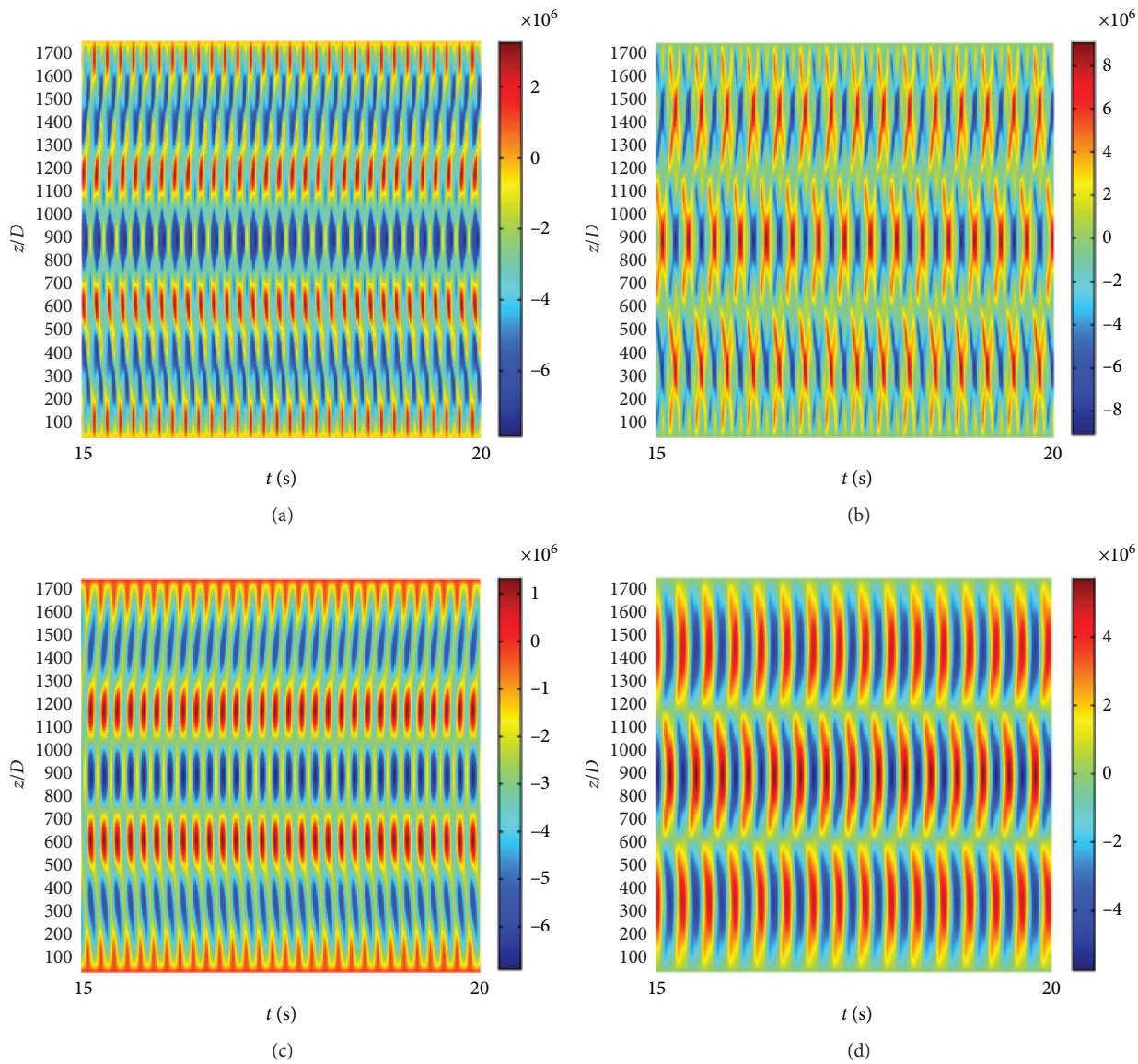

Figure 9: Space-time response of stress under different viscoelastic coefficients. (a) The in-line and (b) cross-flow with $a = 0.001$. (c) The in-line and (d) cross-flow with $a = 0.11$.

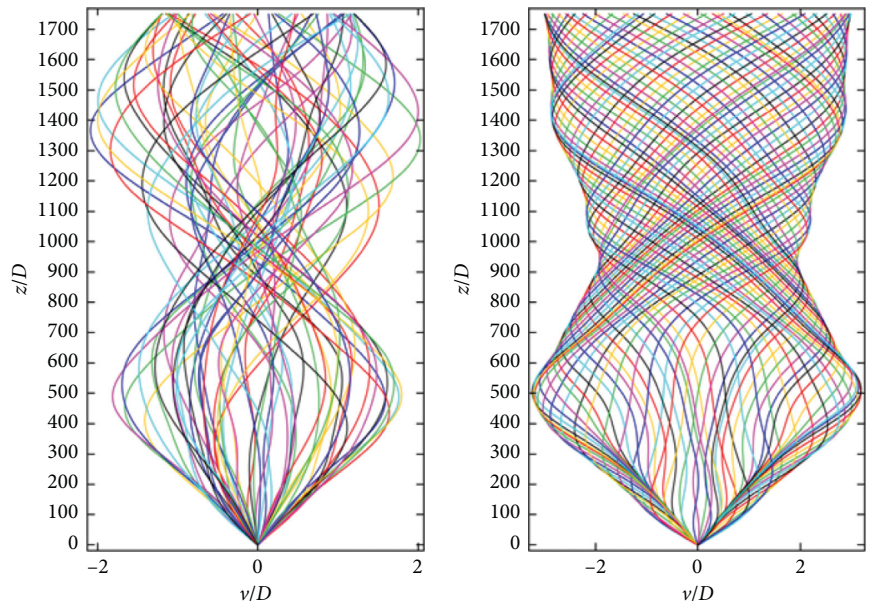

Figure 10: The influences of axial tension excitation amplitude on the displacement response of cross-flow for an (a) excitation amplitude $A/D = 1.2$ and (b) excitation amplitude $A/D = 3.0$.

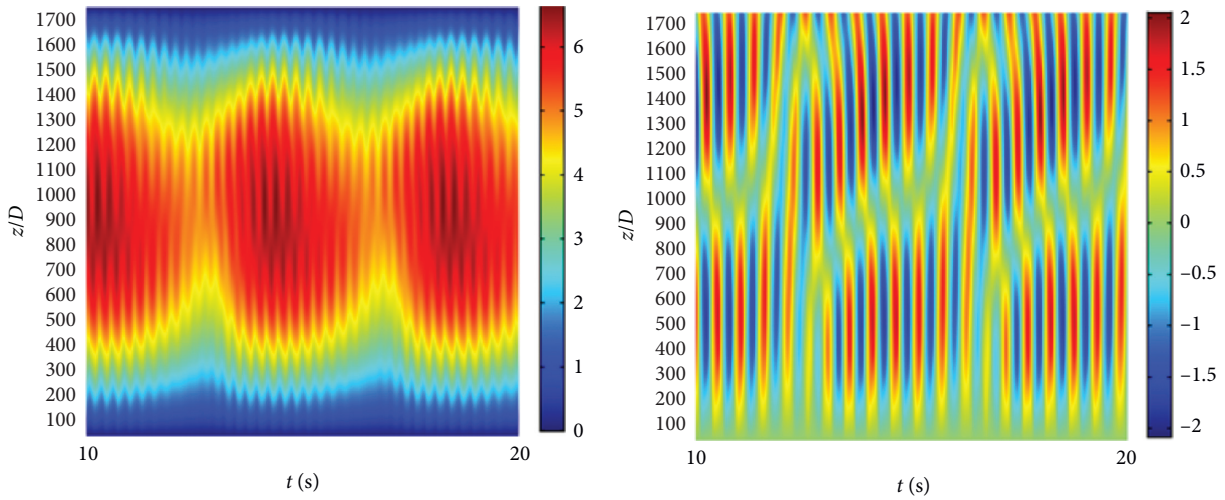

Figure 11: Continued.

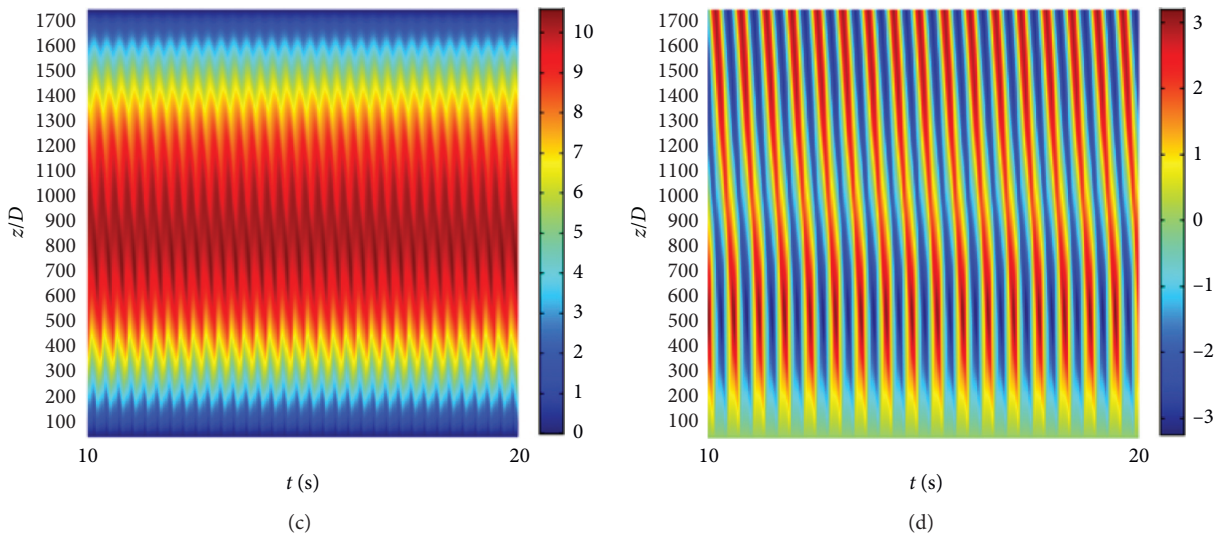

Figure 11: Space-time response of displacement under different axial tension excitation amplitudes. (a) The in-line and (b) cross-flow with $A/D = 1.2$. (c) The in-line and (d) cross-flow with $A/D = 3.0$.

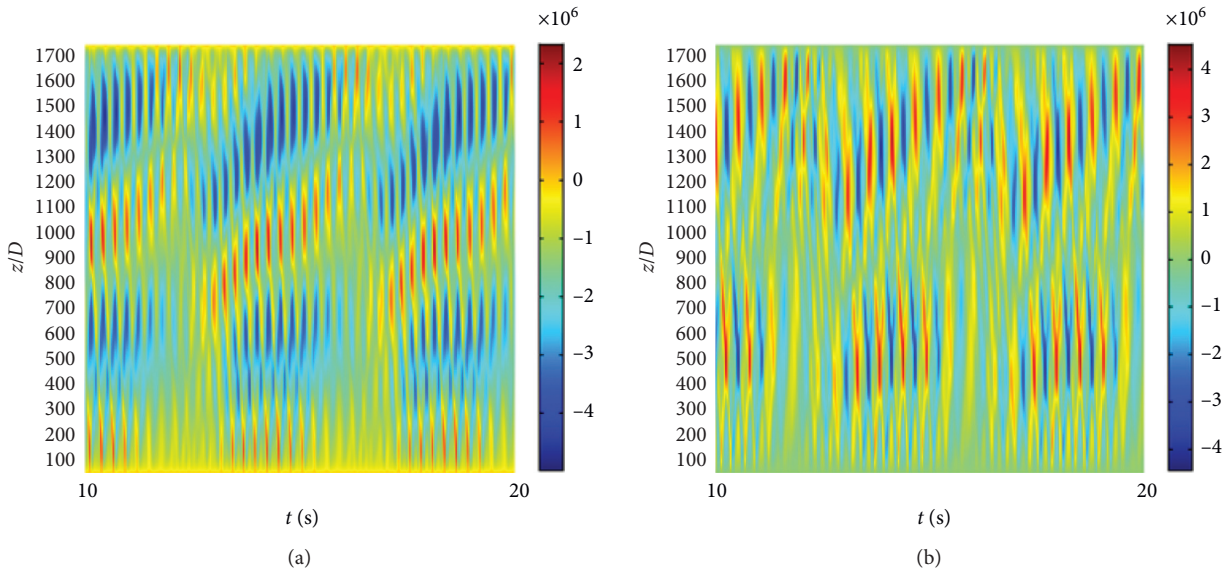

Figure 12: Continued.

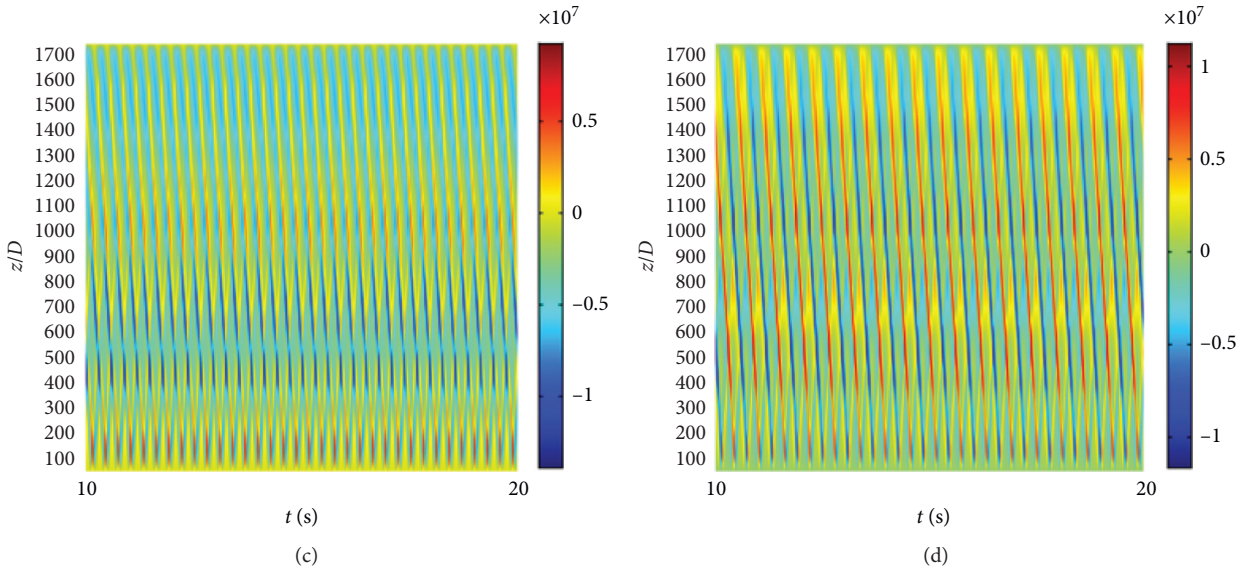

Figure 12: Space-time response of stress of the marine riser under different axial tension excitation amplitudes. (a) The in-line and (b) cross-flow with $A/D = 1.2$. (c) The in-line and (d) cross-flow with $A/D = 3.0$.

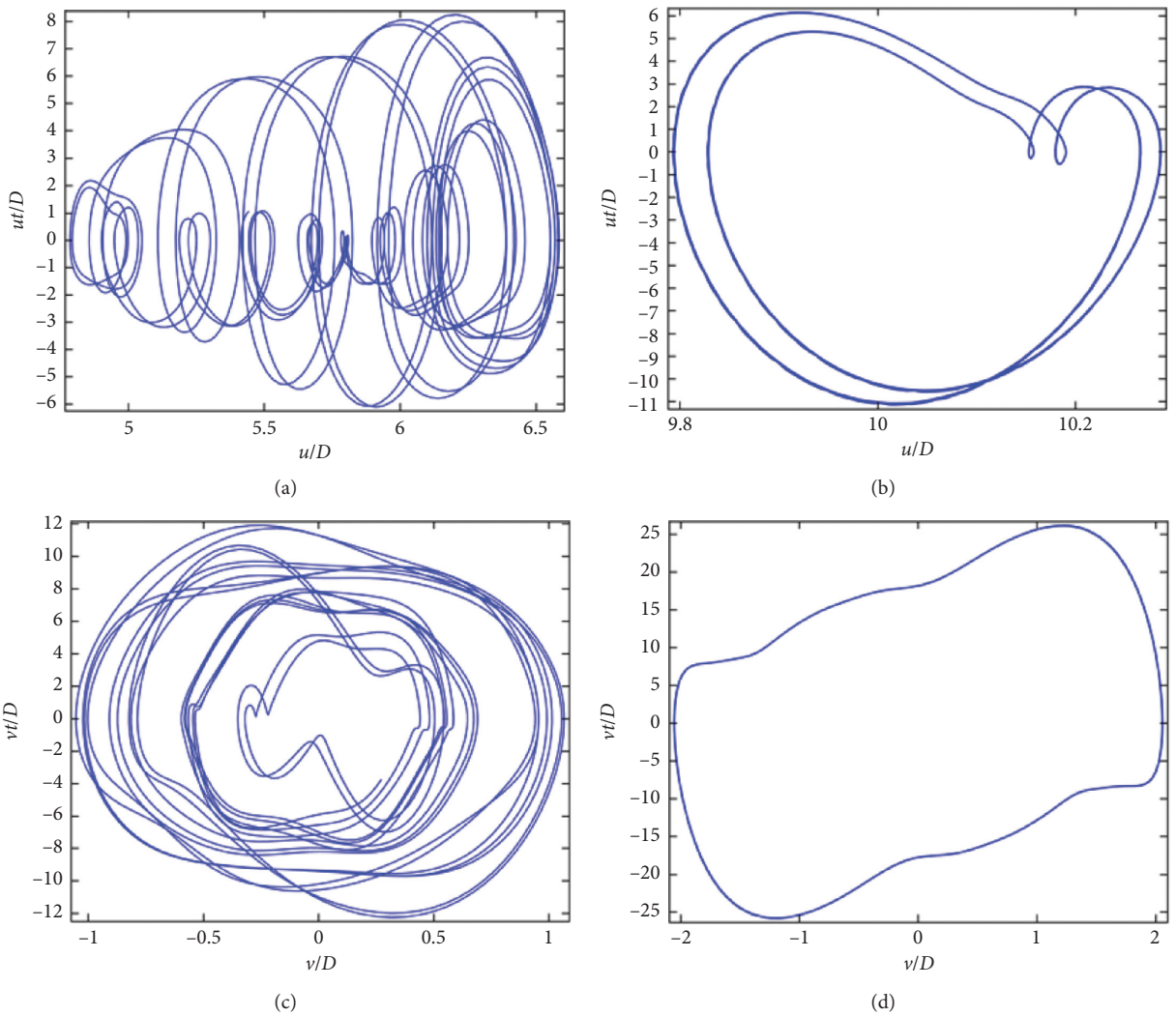

Figure 13: The phase diagram of the marine riser considering the coupling effect: the phase diagram of the in-line with (a) $A/D = 1.2$ and (b) $A/D = 3.0$ and the phase diagram of the cross-flow with (c) $A/D = 1.2$ and (d) $A/D = 3.0$.

respectively, while Figures 9(c) and 9(d) are the stress responses of the in-line and cross-flow under the condition that $a = 0.11$, respectively. It can be viewed that the absolute value of the three-direction maximum stress decreases with the increase of the viscoelastic coefficient and the three-direction maximum stress is symmetrically distributed along the axial direction of the marine riser. The spatial-temporal distribution of stress in the riser varies with the change of the viscoelastic coefficient. The stress distribution in both the in-line and the cross-flow directions shows that the spatial-temporal region of maximum stress increases with the increase of viscoelastic coefficients. The results show that the maximum stress and stress amplitude of the marine riser can be effectively reduced with the increase of viscoelasticity of the riser at low sea water flow velocity.

4.4. Effects of Axial Tension Amplitude on the Vibration Response Characteristics. The influences of axial tension amplitude on the vibration response characteristics of marine riser considering the in-line and cross-flow coupling effect are discussed in this section. The cross-flow displacement response curve under different axial tension excitation amplitudes and different time intervals is displayed in Figure 10, where the axial tension excitation amplitudes in Figure 10(a) are $A/D = 1.2$, while that in Figure 10(b) are $A/D = 3.0$. It can be indicated that the cross-flow displacement response of the riser is dominated by the outflow excitation at low amplitude excitation; however, the displacement response of the riser is dominated by the axial tension excitation when the axial tension amplitude excitation increases to a certain degree.

The space-time response characteristic curves of displacement of the marine riser under different axial tension excitation amplitudes are plotted in Figure 11, where Figures 11(a) and 11(b) are the displacement responses of the in-line and cross-flow under the condition that $A/D = 1.2$, respectively, while Figures 11(c) and 11(d) are displacement responses of the in-line and cross-flow under the condition that $A/D = 3.0$, respectively. It can be viewed from the in-line displacement results that the displacement distribution along the axis direction of the riser and the displacement amplitude change greatly with time and the distribution is asymmetrical under condition that $A/D = 1.2$, while the displacement distribution along the axis direction of the riser changes little with time and the distribution is antiasymmetric and the displacement response tends to periodic movement from the top of the riser to the lower part of the riser under the condition that $A/D = 3.0$.

The results of cross-flow displacement in Figure 11 show that the cross-flow displacement at the top of the riser oscillates periodically according to the given boundary conditions. Due to the influence of the multimode response, the displacement response of the riser in the cross-flow is relatively complex and it is presented as the second-order modal response and a certain periodicity in a large time range under the condition that $A/D = 1.2$. However, the displacement response along the direction of the riser shows a lag. The displacement response of the riser is relatively regular, which is greatly affected by the axial tension excitation under the condition that $A/D = 3.0$. The results of axial displacement show that the axial displacement of the riser presents strong asymmetry at low amplitude and tends to be symmetric at high amplitude.

The space-time response characteristic curves of stress under different axial tension excitation amplitudes are plotted in Figure 12, where Figures 12(a) and 12(b) are stress responses of the in-line and cross-flow under the condition that $A/D = 1.2$, respectively, while Figures 12(c) and 12(d) are stress responses of the in-line and cross-flow under the condition that $A/D = 3.0$, respectively. It can be viewed that the maximum stress of the riser in the in-line and the cross-flow will change in a larger range along the axial direction of the riser under the condition that $A/D = 1.2$. The maximum stress of the riser approximately changes periodically along the axis direction of the riser with time, and the axial stress increases sharply, but the variation amplitude decreases relatively under the condition that $A/D = 3.0$. Therefore, when the axial tension excitation amplitude is large enough, the three-direction stress will increase a lot.

In Figure 13, the phase diagram of the in-line and cross-flow displacement trajectories of the axial center of the marine riser considering the coupling effect is displayed, where the curves in Figures 13(a) and 13(b) are the in-line displacement trajectories of the marine riser, while the ones in Figures 13(c) and 13(d) are the cross-flow displacement trajectories of the marine riser. It is obvious that motions of the marine riser in both the in-line and the cross-flow are aperiodic under the condition that $A/D = 1.2$, while the in-line displacement trajectory is two intersecting "heart-"shaped trajectories and the cross-flow phase displacement trajectory is an inclined square under the condition that $A/D = 3.0$.

4.5. Effects of Gas-Phase Volume Fraction on the Vibration Response Characteristics. The influences of gas-phase volume fraction on the vibration response characteristics of the marine riser considering the in-line and cross-flow coupling effect are discussed in this section.

For some prescribed values of different gas-phase volume fractions, the response characteristic curves of the cross-flow displacement response of the marine riser versus different gas-phase volume fractions with $U = 0.3$ m/s and $\varepsilon_g = 0$, 0.7, and 0.8 are plotted in Figure 14, where different color curves in the figure represent the cross-flow displacement response of the riser with the same time interval. It can be viewed that the cross-flow response mode of the riser is four orders under the condition that $\varepsilon_g = 0$, while the cross-flow response mode of the riser is a transition from the 4th-order mode to the 3rd-order mode under the condition that $\varepsilon_g = 0.7$, and the cross-flow response mode of the riser is three orders under the condition that $\varepsilon_g = 0.8$.

The space-time response characteristic curves of displacement of the marine riser under different gas-phase volume fractions are plotted in Figure 15, where Figures 15(a), 15(c), and 15(e) are the in-line displacement responses under the condition that $\varepsilon_g = 0$, $\varepsilon_g = 0.7$, and $\varepsilon_g = 0.8$, respectively, while Figures 15(b), 15(d), and 15(f)

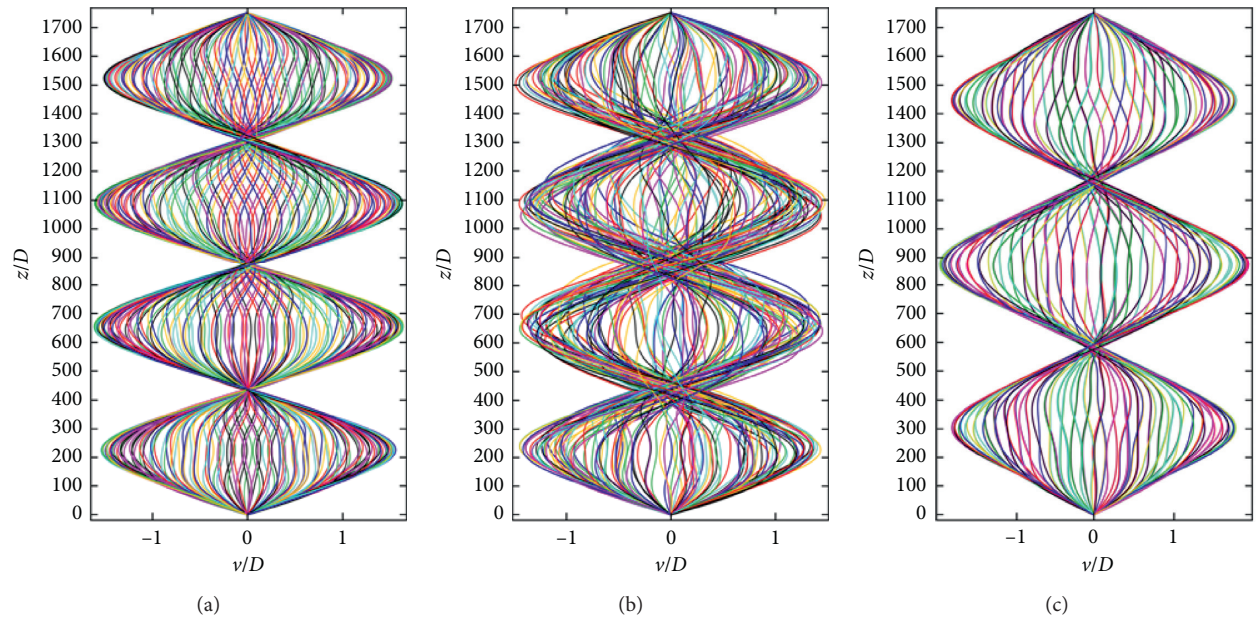

Figure 14: Vibration response modes under the condition of different gas-phase volume fractions with (a) $\varepsilon_g = 0$, (b) $\varepsilon_g = 0.7$, and (c) $\varepsilon_g = 0.8$.

are the cross-flow displacement responses under the condition that $\varepsilon_g = 0$, $\varepsilon_g = 0.7$, and $\varepsilon_g = 0.8$, respectively. It can be viewed that the response of the two-dimensional displacement of the riser is similar under the condition that $\varepsilon_g = 0$ and $\varepsilon_g = 0.8$, and the space-time response of the displacement of the marine riser is mainly in the form of a standing wave. However, the cross-flow displacement of the riser responds in mode 4 under the condition that $\varepsilon_g = 0$, while the cross-flow displacement of the riser responds in mode 3 under the condition that $\varepsilon_g = 0.8$. The space-time response of the two-dimensional displacement of the riser is shown as the superposition state of standing wave and traveling wave under the condition that $\varepsilon_g = 0.7$ and the cross-flow displacement of the marine riser responds in mode of 4 order.

The space-time response characteristic curves of the in-line and cross-flow stress of the marine riser under different gas-phase volume fractions are plotted in Figure 16, where Figures 16(a), 16(c), and 16(e) are the in-line stress responses of marine riser under the condition that $\varepsilon_g = 0$, $\varepsilon_g = 0.7$, and $\varepsilon_g = 0.8$, respectively, while Figures 16(b), 16(d), and 16(f) are the cross-flow stress responses of the marine riser under the condition that $\varepsilon_g = 0$, $\varepsilon_g = 0.7$, and $\varepsilon_g = 0.8$, respectively. It can be viewed that the in-line and cross-flow stress of the riser vary regularly with time under the condition that $\varepsilon_g = 0$ and $\varepsilon_g = 0.8$. In addition, the stress distribution along the direction of the riser is symmetrical and the stresses are mainly in the form of standing wave. While the stress distribution along the direction of the riser is asymmetric, the space-time response of the in-line and cross-flow stress of the riser is shown as the superposition state of standing waves and traveling waves.

In Figure 17, the characteristic relationship curves of the displacement trajectories along different axial positions of the marine riser with different gas-phase volume fractions are displayed, where the curves in Figures 17(a), 17(c), and 17(e) are the displacement trajectories of the marine riser with $\varepsilon_g = 0$, while the ones in Figures 17(b), 17(d), and 17(f) are the displacement trajectories of the marine riser with $\varepsilon_g = 0.8$. It is obvious that the displacement trajectory of the riser is close to a single closed curve, but the displacement trajectory along the axial symmetric position of the riser is no longer symmetric. In addition, the displacement trajectories of the marine riser in the x-y and y-z planes are mainly in the shape of "8," while the displacement trajectories in the x-z plane are mainly in the shape of a ring. The phase trajectories in Figures 17(e) and 17(f) are a mixture of "8" shape and "crescent" shape, and the phase trajectories near the center of the riser are "crescent" shaped and near both ends of the riser are "8" shaped.

The displacement-time response characteristic curves of the axial center of the marine riser under different gas-phase volume fractions are plotted in Figures 18, where Figures 18(a), 18(c), and 18(e) are the in-line displacement-time responses of the marine riser under the condition that $\varepsilon_g = 0$, $\varepsilon_g = 0.8$, and $\varepsilon_g = 0.8$, respectively, while Figures 18(b), 18(d), and 18(f) are the cross-flow displacement-time responses of the marine riser under the condition that $\varepsilon_g = 0$, $\varepsilon_g = 0.8$, and $\varepsilon_g = 0.8$, respectively. It can be viewed that the motion is close to periodic motion under the condition that $\varepsilon_g = 0$ and $\varepsilon_g = 0.8$, while the in-line and cross-flow displacement response of the marine riser show a strong aperiodic property under the condition that $\varepsilon_g = 0.7$. In addition, there is a large "jump" in the cross-flow displacement response; the cross-flow displacement response shows the superposition state of multiple harmonics, and the axial displacement response shows a "locking" interval. Moreover, the nonlinear response of the marine riser is

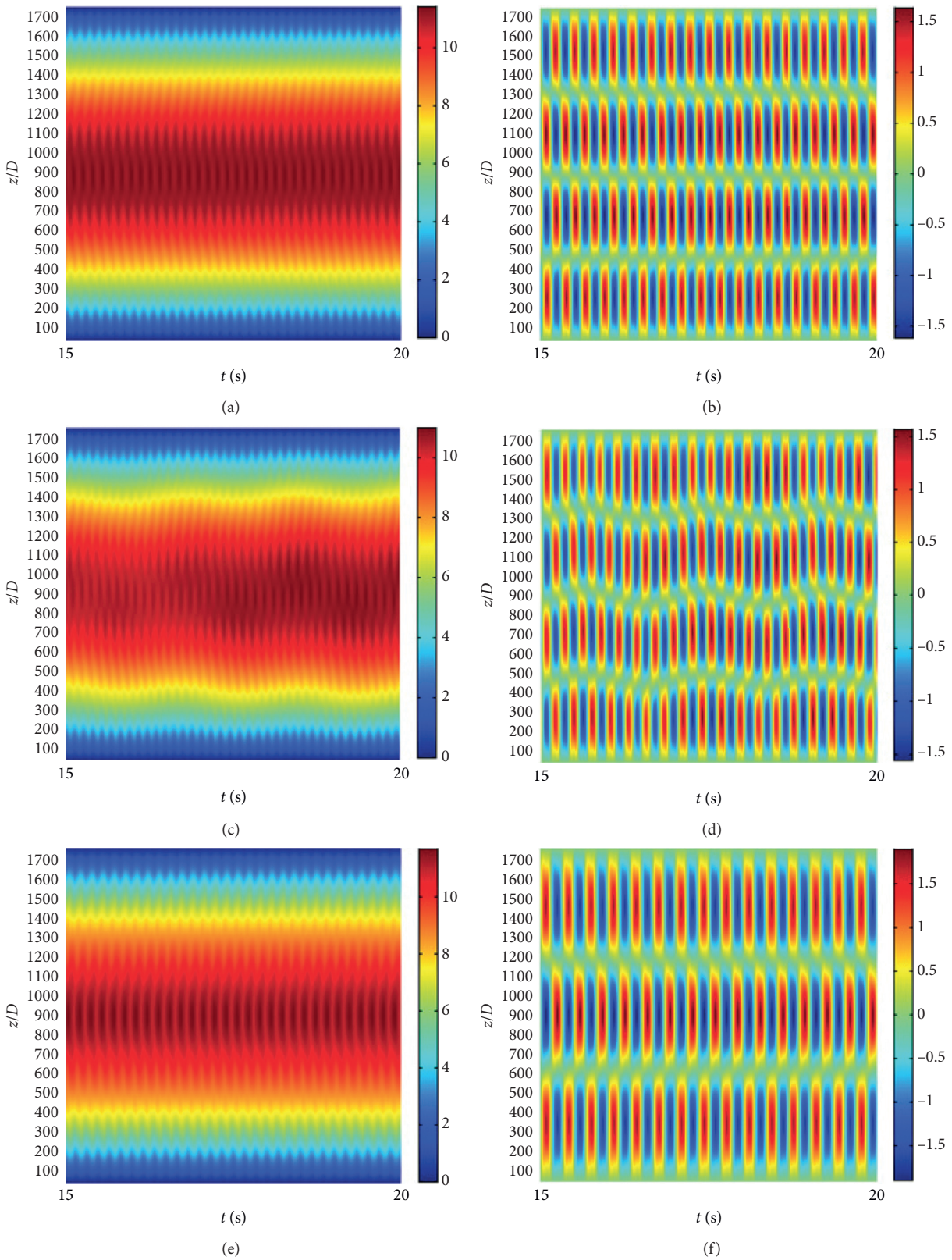

Figure 15: Space-time response of displacement under different gas-phase volume fractions. (a) The in-line and (b) cross-flow with $\varepsilon_g = 0$. (c) The in-line and (d) cross-flow with $\varepsilon_g = 0.7$. (e) The in-line and (f) cross-flow with $\varepsilon_g = 0.8$.

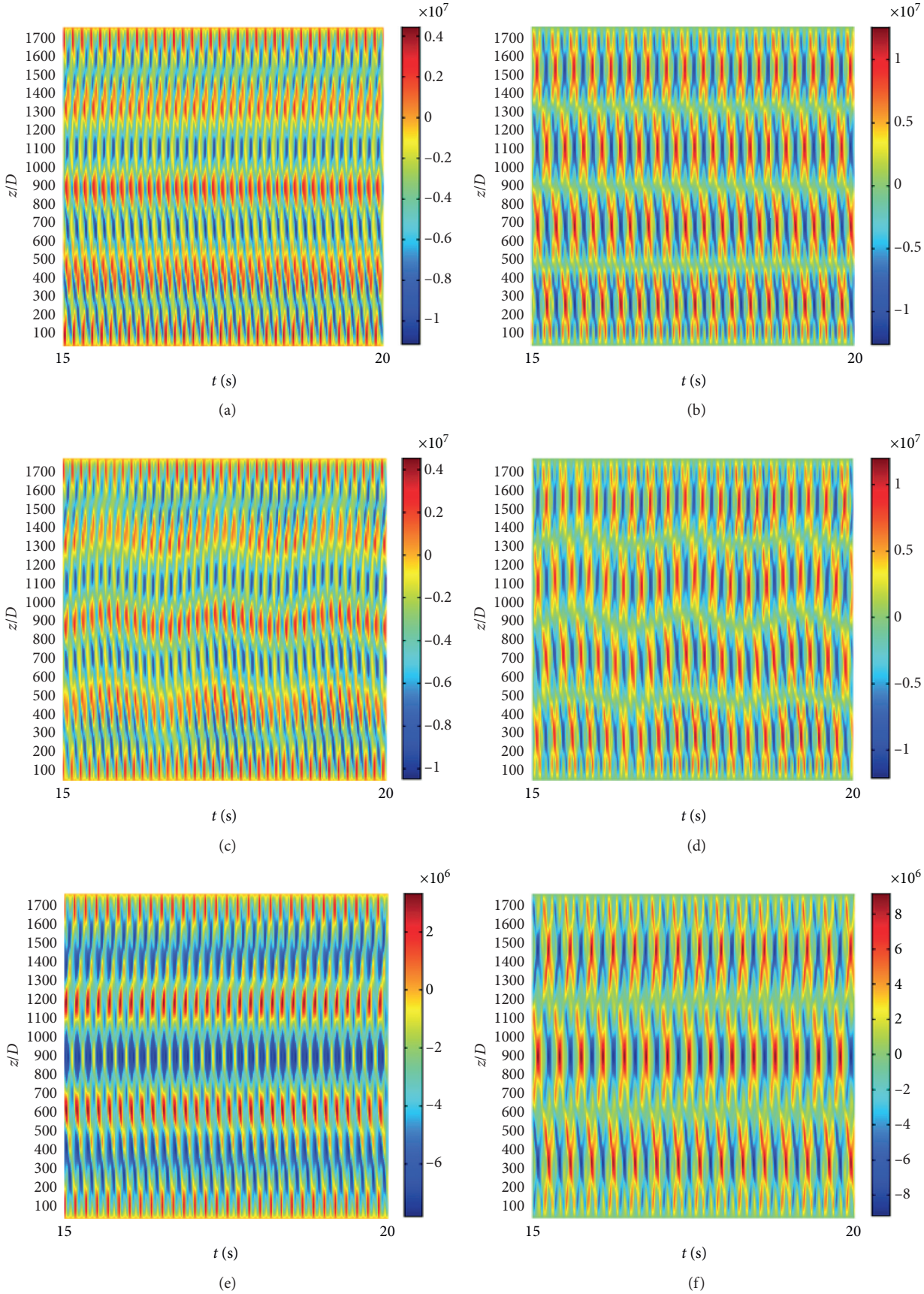

FIGURE 16: Space-time response of stress of the marine riser under different gas-phase volume fractions. (a) The in-line and (b) cross-flow with $\varepsilon_g = 0$. (c) The in-line and (d) cross-flow with $\varepsilon_g = 0.7$. (e) The in-line and (f) cross-flow with $\varepsilon_g = 0.8$.

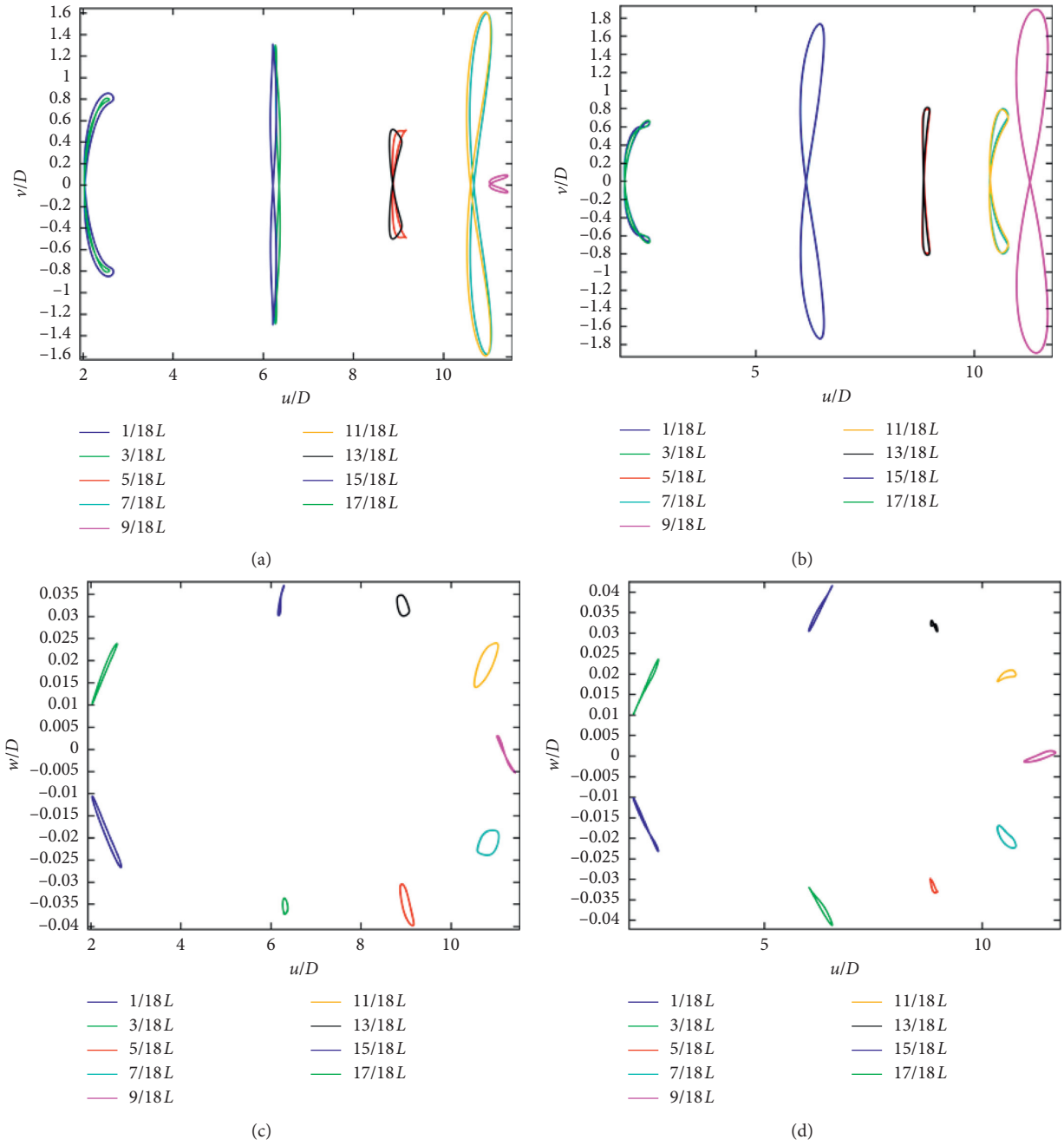

Figure 17: Continued.

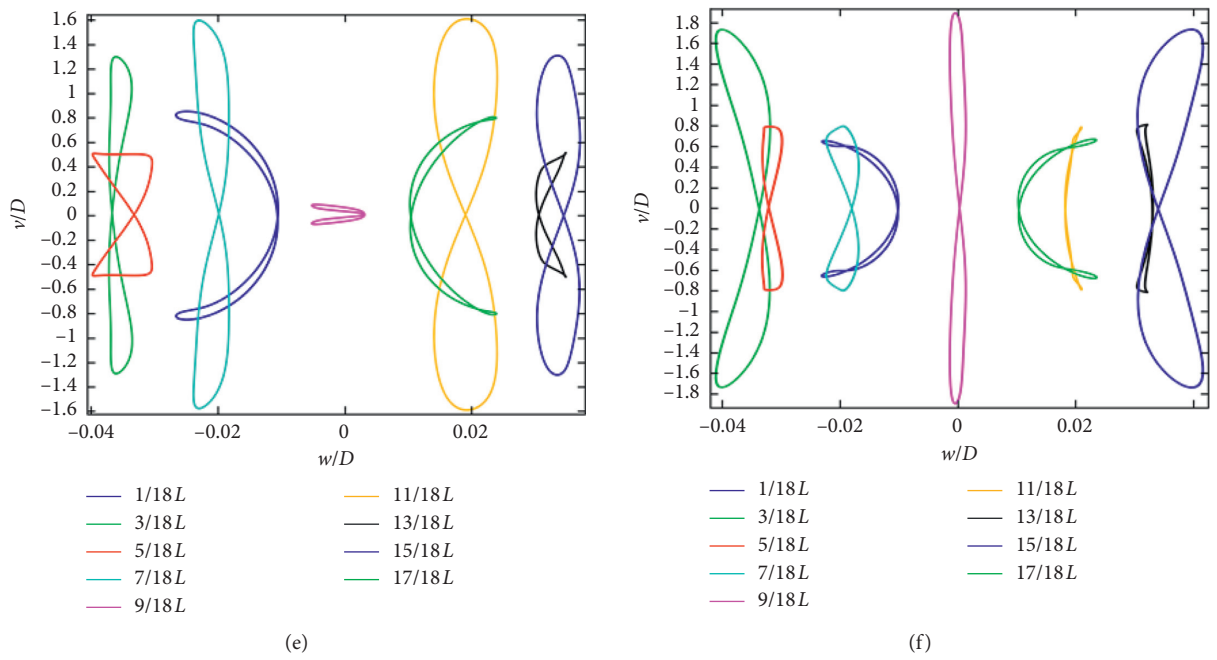

Figure 17: The displacement trajectories of the marine riser at different gas-phase volume fractions in the x-y plane with (a) $\varepsilon_g = 0$ and (b) $\varepsilon_g = 0.8$, in the x-z plane with (c) $\varepsilon_g = 0$ and (d) $\varepsilon_g = 0.8$, and in the y-z plane with (e) $\varepsilon_g = 0$ and (f) $\varepsilon_g = 0.8$.

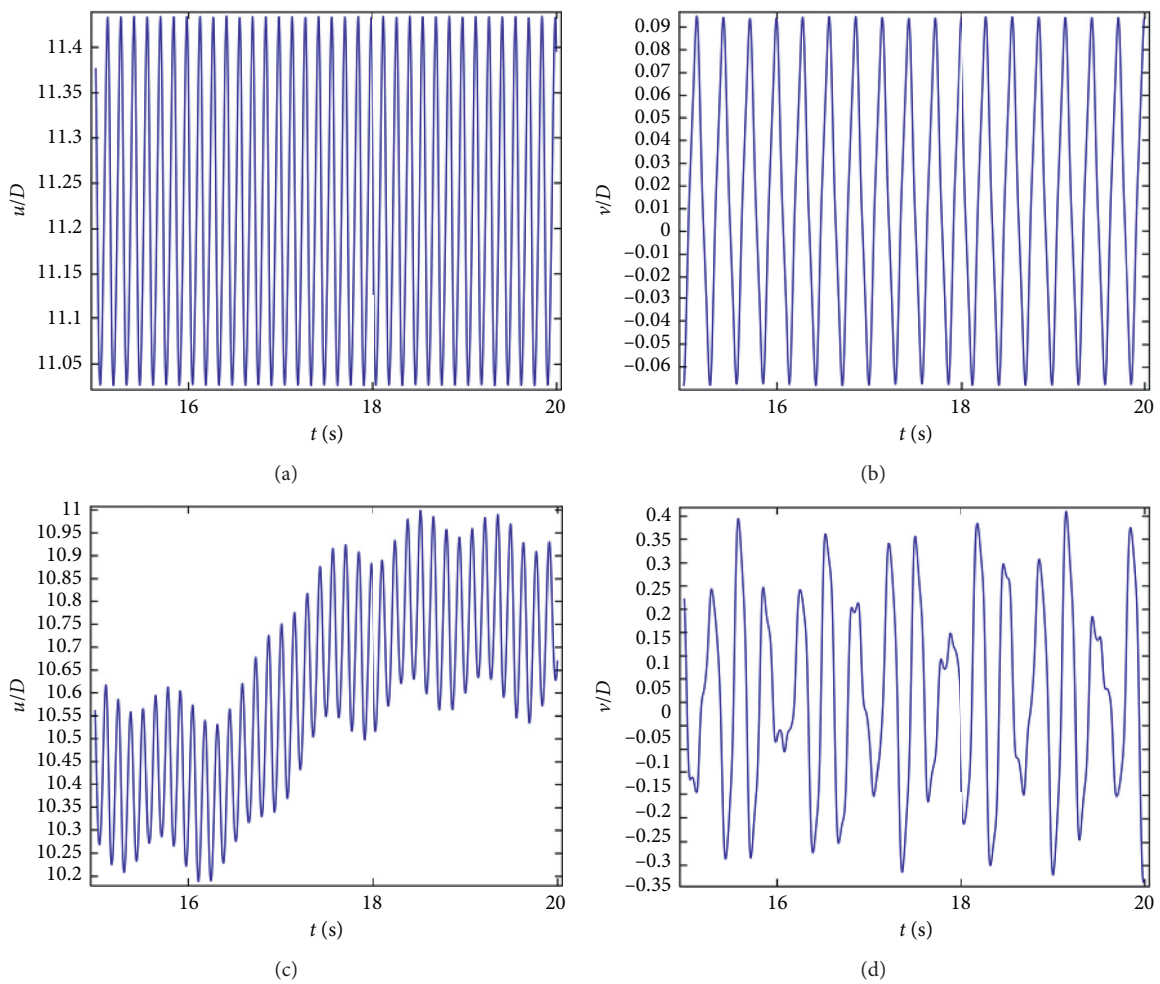

Figure 18: Continued.

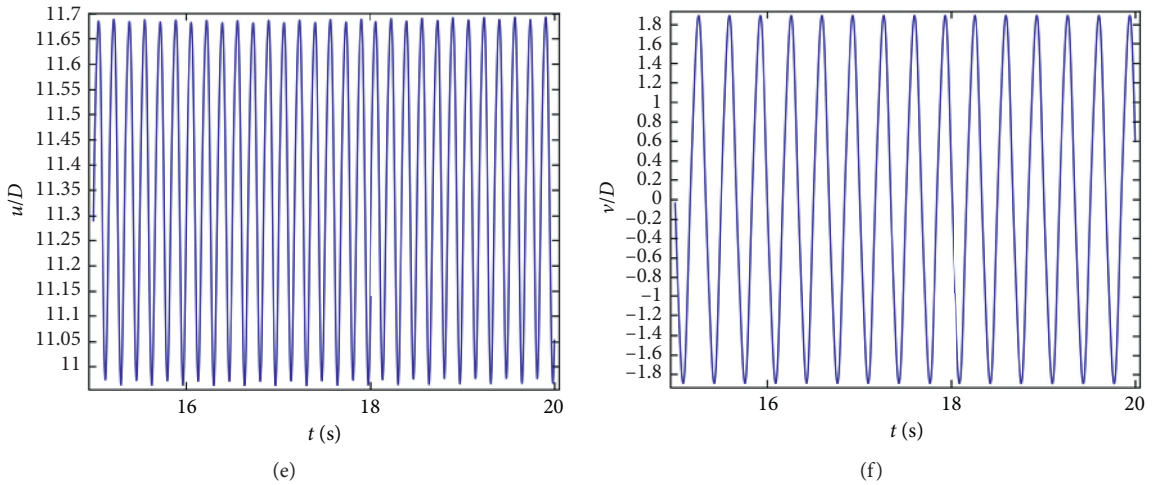

(e) (f)

Figure 18: Displacement response at the axial center of the marine riser under the condition of different gas-phase volume fractions. (a) The in-line and (b) cross-flow with $\varepsilon_g = 0$. (c) The in-line and (d) cross-flow with $\varepsilon_g = 0.7$. (e) The in-line and (f) cross-flow with $\varepsilon_g = 0.8$.

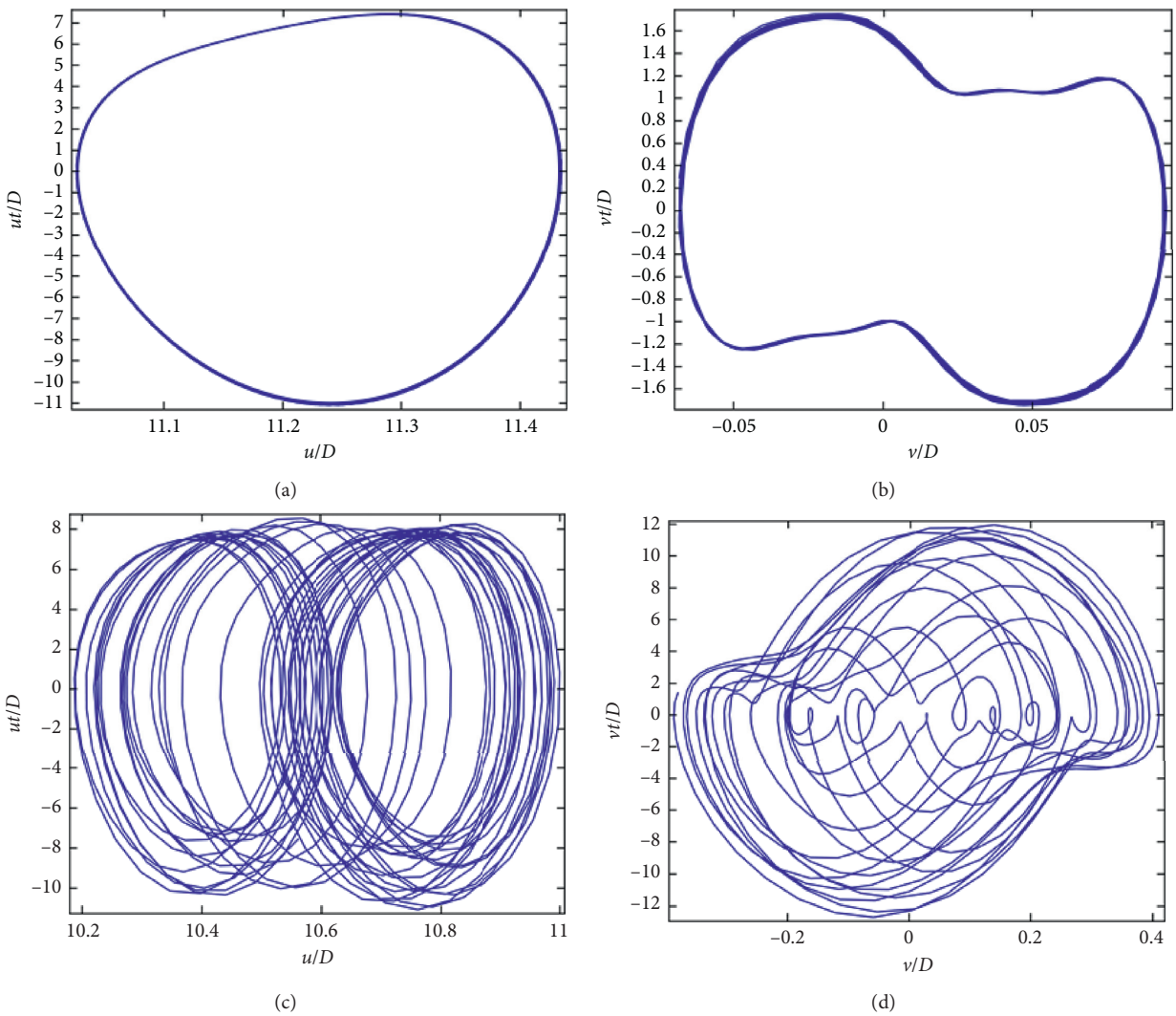

(a) (b)

(c) (d)

Figure 19: Continued.

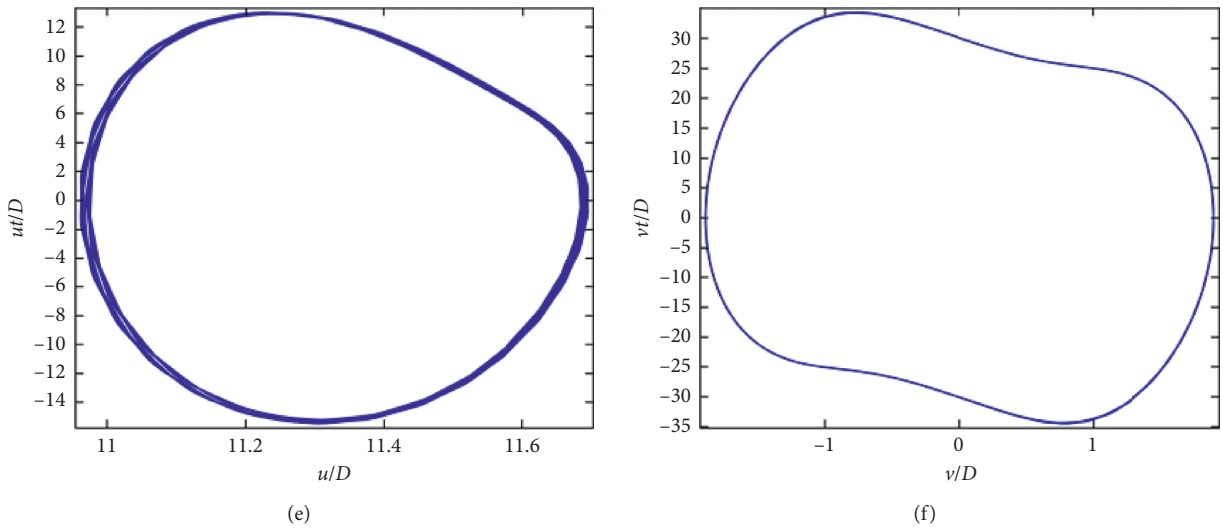

Figure 19: The phase diagram at the axial center of the marine riser under the condition of different gas-phase volume fractions considering the coupling effect: the phase diagram of (a) the in-line and (b) cross-flow with $\varepsilon_g = 0$, (c) the in-line and (d) cross-flow with $\varepsilon_g = 0.7$, and (e) the in-line and (f) cross-flow with $\varepsilon_g = 0.8$.

intensified when the gas-phase volume fraction makes the riser near the critical point of "jumping" in the cross-flow mode.

In Figure 19, the phase diagram of the in-line and cross-flow displacement trajectories of the axial center of the marine riser considering the coupling effect is displayed, where the curves in Figures 19(a), 19(c), and 19(e) are the in-line displacement trajectories of the marine riser under the condition that $\varepsilon_g = 0$, $\varepsilon_g = 0.8$, and $\varepsilon_g = 0.8$, respectively, while the curves in Figures 19(b), 19(d), and 19(f) are the cross-flow displacement trajectories of the marine riser under the condition that $\varepsilon_g = 0$, $\varepsilon_g = 0.8$, and $\varepsilon_g = 0.8$, respectively. It is obvious that the phase trajectory is close to a single closed curve under the condition that $\varepsilon_g = 0$ and $\varepsilon_g = 0.8$, while the phase trajectory is more complex and shows aperiodic motion under the condition that $\varepsilon_g = 0.7$.

5. Conclusions

The in-line and cross-flow coupling vibration response characteristics of a marine viscoelastic riser subjected to two-phase internal flow taking into account both the geometric and hydrodynamic nonlinearities are presented in this paper. Extended Hamilton's principle is employed to obtain the dynamic equations. Two distributed and coupled van der Pol wake oscillators are utilized to model the fluctuating lift and drag coefficients, respectively. Employing the finite element method, the in-line and cross-flow coupling vibration response characteristics of systems are derived. The combined effects of multiple factors on the in-line and cross-flow coupling vibration response characteristics of the marine viscoelastic riser are systematically discussed. Specifically, the combined influences of the volume fraction of gas phase, sea water flow velocity, viscoelastic coefficient of the marine riser, axial tension amplitude, the in-line and cross-flow coupling effect, multiphase internal flow velocity on the in-line and cross-flow vibration pattern, the in-line and cross-flow displacement trajectories, the in-line and cross-flow space-time response of displacement, and the in-line and cross-flow space-time response of stress of structures are investigated. The results show that the orbital motions showed the IL-CF and IL-CF trajectories dominate figure-of-eight shapes, and the IL-AX trajectories depict a majority of "O" shapes. The phase diagram of the IL and CF directions depicted that the dynamic responses behaved as periodic and aperiodic responses depending on internal flow velocity. Furthermore, the maximum displacements and stresses of the marine viscoelastic riser can be increased or decreased depending on the internal flow velocity, and the discontinuous jumping phenomenon of the in-line response modal is discovered.

Data Availability

Data used to support the findings of this study can be obtained from the corresponding author on request.

Additional Points

Summary: owing to the lack of VIV experiment concerned with internal flow, model validations are firstly performed through comparisons with the published experiment and numerical simulation results. Previous prediction results concluded by Zanganeh and Srinil [38] have highlighted the importance of considering the axial dynamic coupling, the amplification of IL mean displacements, and the geometric and hydrodynamic nonlinearities. Therefore, variations of maximum IL and CF displacement amplitudes of the flexible riser with respect to cross-flow velocity are plotted in Figure 2 for different analysis methods. It is found that the IL displacement amplitudes between experiment and numerical simulations agree very well at lower cross-flow velocity.

Outside this region of cross-flow velocity, the IL displacement amplitudes obtained by experiment keep almost larger than numerical simulations. It indicates that the present solution is very close to the experimental result, which validates the present solution.

Conflicts of Interest

The authors declare that they have no conflicts of interest.

Acknowledgments

This research work was supported by the National Natural Science Foundation of China (Nos. 51674216, 11702230, and 11602208). This research was also supported by the Open Fund (OGE201702-26) of Key Laboratory of Oil & Gas Equipment, the Ministry of Education (Southwest Petroleum University).

References

[1] X. Han, W. Lin, A. Qiu et al., "Understanding vortex-induced vibration characteristics of a long flexible marine riser by a bidirectional fluid-structure coupling method," *Journal of Marine Science and Technology*, vol. 25, no. 2, pp. 620–639, 2020.

[2] M. Lou, G. Qian, and R. Li, "Experimental investigation of the suppression of vortex-induced vibration in four cylinders arranged in a square under different spacing ratios," *Journal of Marine Science and Technology*, vol. 25, no. 2, pp. 467–481, 2020.

[3] W. Yang, Z. Ai, X. Zhang, R. Gou, and X. Chang, "Nonlinear three-dimensional dynamics of a marine viscoelastic riser subjected to uniform flow," *Ocean Engineering*, vol. 149, pp. 38–52, 2018.

[4] H.-l. Gu, H.-y. Guo, Z. Liu, F.-h. Li, W.-b. An, and P. Li, "Experimental study and fatigue analysis of vortex-induced vibration of umbilical cable considering internal friction," *China Ocean Engineering*, vol. 34, no. 2, pp. 151–161, 2020.

[5] Y. Wang, Z. Wu, G. Zhang, Y. Li, and F. Wang, "Bifurcation phenomenon and multi-stable behavior in vortex-induced vibration of top tension riser in shear flow," *Journal of Vibration and Control*, vol. 26, no. 9-10, pp. 659–670, 2020.

[6] P. W. Bearman, "Circular cylinder wakes and vortex-induced vibrations," *Journal of Fluids and Structures*, vol. 27, no. 5-6, pp. 648–658, 2011.

[7] R. D. Gabbai and H. Benaroya, "An overview of modeling and experiments of vortex-induced vibration of circular cylinders," *Journal of Sound and Vibration*, vol. 282, no. 3-5, pp. 575–616, 2005.

[8] C. H. K. Williamson and R. Govardhan, "Vortex-induced vibrations," *Annual Review of Fluid Mechanics*, vol. 36, no. 1, pp. 413–455, 2004.

[9] F. J. Huera-Huarte and P. W. Bearman, "Wake structures and vortex-induced vibrations of a long flexible cylinder-part 1: dynamic response," *Journal of Fluids and Structures*, vol. 25, no. 6, pp. 969–990, 2009.

[10] N. Srinil, "Multi-mode interactions in vortex-induced vibrations of flexible curved/straight structures with geometric nonlinearities," *Journal of Fluids and Structures*, vol. 26, no. 7-8, pp. 1098–1122, 2010.

[11] N. Srinil, "Analysis and prediction of vortex-induced vibrations of variable-tension vertical risers in linearly sheared currents," *Applied Ocean Research*, vol. 33, no. 1, pp. 41–53, 2011.

[12] X. Wu, F. Ge, and Y. Hong, "A review of recent studies on vortex-induced vibrations of long slender cylinders," *Journal of Fluids and Structures*, vol. 28, pp. 292–308, 2012.

[13] T. Ueno and G. R. Franzini, "Numerical studies on passive suppression of one and two degrees-of-freedom vortex-induced vibrations using a rotative non-linear vibration absorber," *International Journal of Non-Linear Mechanics*, vol. 116, pp. 230–249, 2019.

[14] A. Postnikov, E. Pavlovskaia, and M. Wiercigroch, "2DOF CFD calibrated wake oscillator model to investigate vortex-induced vibrations," *International Journal of Mechanical Sciences*, vol. 127, pp. 176–190, 2017.

[15] N. Srinil and H. Zanganeh, "Modelling of coupled cross-flow/in-line vortex-induced vibrations using double Duffing and van der Pol oscillators," *Ocean Engineering*, vol. 53, pp. 83–97, 2012.

[16] H. Zanganeh and N. Srinil, "Characterization of variable hydrodynamic coefficients and maximum responses in two-dimensional vortex-induced vibrations with dual resonances," *Journal of Vibration & Acoustics*, vol. 136, pp. 51–84, 2014.

[17] N. Srinil and G. Rega, "Two-to-one resonant multi-modal dynamics of horizontal/inclined cables. Part II: internal resonance activation, reduced-order models and nonlinear normal modes," *Nonlinear Dynamics*, vol. 48, no. 3, pp. 253–274, 2007.

[18] G. Ricciardi and F. Saitta, "A continuous vibration analysis model for cables with sag and bending stiffness," *Engineering Structures*, vol. 30, no. 5, pp. 1459–1472, 2008.

[19] B. Sanaati and N. Kato, "A study on the effects of axial stiffness and pre-tension on VIV dynamics of a flexible cylinder in uniform cross-flow," *Applied Ocean Research*, vol. 37, pp. 198–210, 2012.

[20] J. R. Chaplin, P. W. Bearman, F. J. Huera Huarte, and R. J. Pattenden, "Laboratory measurements of vortex-induced vibrations of a vertical tension riser in a stepped current," *Journal of Fluids and Structures*, vol. 21, no. 1, pp. 3–24, 2005.

[21] W. Xu, Y. Ma, C. Ji, and C. Sun, "Laboratory measurements of vortex-induced vibrations of a yawed flexible cylinder at different yaw angles," *Ocean Engineering*, vol. 154, pp. 27–42, 2018.

[22] G. R. Franzini, C. P. Pesce, R. Salles, R. T. Gonçalves, A. L. C. Fujarra, and P. Mendes, "Experimental analysis of a vertical and flexible cylinder in water: response to top motion excitation and parametric resonance," *Journal of Vibration & Acoustics*, vol. 137, pp. 31–64, 2014.

[23] F. He, H. Dai, and L. Wang, "Vortex-induced vibrations of a pipe subjected to unsynchronized support motions," *Journal of Marine Science and Technology*, vol. 23, no. 4, pp. 978–990, 2018.

[24] T. Jiang, Z. Liu, H. Dai, L. Wang, and F. He, "Nonplanar multi-modal vibrations of fluid-conveying risers under shear cross flows," *Applied Ocean Research*, vol. 88, pp. 187–209, 2019.

[25] H. L. Dai, L. Wang, Q. Qian, and Q. Ni, "Vortex-induced vibrations of pipes conveying fluid in the subcritical and supercritical regimes," *Journal of Fluids and Structures*, vol. 39, no. 5, pp. 322–334, 2013.

[26] M. C. Rahmani, A. Kaci, A. A. Bousahla et al., "Influence of boundary conditions on the bending and free vibration behavior of FGM sandwich plates using a four-unknown refined integral plate theory," *Computers and Concrete*, vol. 25, no. 3, pp. 225–244, 2020.

[27] A. A. Bousahla, F. Bourada, S. R. Mahmoud, A. Tounsi, A. Algarni, and E. A. A. Bedia, "Buckling and dynamic behavior of the simply supported CNT-RC beams using an integral-first shear deformation theory," *Computers and Concrete*, vol. 25, no. 2, pp. 155–166, 2020.

[28] M. Kaddari, A. Kaci, A. A. Bousahla et al., "A study on the structural behaviour of functionally graded porous plates on elastic foundation using a new quasi-3D model: bending and Free vibration analysis," *Computers and Concrete*, vol. 25, no. 1, pp. 37–57, 2020.

[29] F. Y. Addou, M. Meradjah, A. A. Bousahla et al., "Influences of porosity on dynamic response of FG plates resting on Winkler/Pasternak/Kerr foundation using quasi 3D HSDT," *Computers and Concrete*, vol. 24, no. 4, pp. 347–367, 2019.

[30] L. A. Chaabane, F. Bourada, M. Sekkal et al., "Analytical study of bending and free vibration responses of functionally graded beams resting on elastic foundation," *Structural Engineering and Mechanics*, vol. 71, no. 2, pp. 185–196, 2019.

[31] L. Boulefrakh, H. Hebali, A. Chikh, A. A. Bousahla, A. Tounsi, and S. R. Mahmoud, "The effect of parameters of visco-Pasternak foundation on the bending and vibration properties of a thick FG plate," *Geomechanics and Engineering*, vol. 18, no. 2, pp. 161–178, 2019.

[32] Z. Boukhlif, M. Bouremana, F. Bourada et al., "A simple quasi-3D HSDT for the dynamics analysis of FG thick plate on elastic foundation," *Steel and Composite Structures*, vol. 31, no. 5, pp. 503–516, 2019.

[33] A. C. Galucio, J.-F. Deü, and R. Ohayon, "Finite element formulation of viscoelastic sandwich beams using fractional derivative operators," *Computational Mechanics*, vol. 33, no. 4, pp. 282–291, 2004.

[34] F. C. L. Borges, N. Roitman, C. Magluta, D. A. Castello, and R. Franciss, "A concept to reduce vibrations in steel catenary risers by the use of viscoelastic materials," *Ocean Engineering*, vol. 77, no. 5, pp. 1–11, 2014.

[35] M. P. Paidoussis, *Fluid-Structure Interactions: Slender Structures and Axial Flow*, Academic Press, Cambridge, MA, USA, 1998.

[36] J. M. Cabrera-Miranda, J. K. Paik, and J. K. Paik, "Two-phase flow induced vibrations in a marine riser conveying a fluid with rectangular pulse train mass," *Ocean Engineering*, vol. 174, pp. 71–83, 2019.

[37] X. P. Chang, X. Li, L. Yang, and Y. H. Li, "Vibration characteristics of the stepped drill string subjected to gas-structure interaction and spinning motion," *Journal of Sound and Vibration*, vol. 450, pp. 251–275, 2019.

[38] S. Meng, X. Zhang, C. Che, and W. Zhang, "Cross-flow vortex-induced vibration of a flexible riser transporting an internal flow from subcritical to supercritical," *Ocean Engineering*, vol. 139, pp. 74–84, 2017.

[39] M. J. Pettigrew and C. E. Taylor, "Two-phase flow-induced vibration: an overview," *Journal of Pressure Vessel Technology*, vol. 116, pp. 1–3, 1994.

[40] C. An and J. Su, "Dynamic behavior of pipes conveying gas-liquid two-phase flow," *Nuclear Engineering and Design*, vol. 292, pp. 204–212, 2015.

[41] T. Ma, J. Gu, and M. Duan, "Dynamic response of pipes conveying two-phase flow based on Timoshenko beam model," *Marine Systems & Ocean Technology*, vol. 6, pp. 1–14, 2017.

[42] C. Monette and M. J. Pettigrew, "Fluidelastic instability of flexible tubes subjected to two-phase internal flow," *Journal of Fluids and Structures*, vol. 19, no. 7, pp. 943–956, 2004.

[43] H. Zanganeh and N. Srinil, "Three-dimensional VIV prediction model for a long flexible cylinder with axial dynamics and mean drag magnifications," *Journal of Fluids and Structures*, vol. 66, pp. 127–146, 2016.

[44] M. L. Facchinetti, E. de Langre, and F. Biolley, "Coupling of structure and wake oscillators in vortex-induced vibrations," *Journal of Fluids and Structures*, vol. 19, no. 2, pp. 123–140, 2004.

[45] J.-n. Song, L. Lu, B. Teng, H.-i. Park, G.-q. Tang, and H. Wu, "Laboratory tests of vortex-induced vibrations of a long flexible riser pipe subjected to uniform flow," *Ocean Engineering*, vol. 38, no. 11-12, pp. 1308–1322, 2011.